Physiol Rev 85: 811–844, 2005;
doi:10.1152/physrev.00022.2004.

Thin and Strong! The Bioengineering Dilemma in the Structural and Functional Design of the Blood-Gas Barrier

JOHN N. MAINA AND JOHN B. WEST

School of Anatomical Sciences, Faculty of Health Sciences, The University of the Witwatersrand, Johannesburg, South Africa; and Department of Medicine, School of Medicine, University of California, San Diego, La Jolla, California

Maina, John N., and John B. West. Thin and Strong! The Bioengineering Dilemma in the Structural and Functional Design of the Blood-Gas Barrier. *Physiol Rev* 85: 811–844, 2005; doi:10.1152/physrev.00022.2004.—In gas exchangers, the tissue barrier, the partition that separates the respiratory media (water/air and hemolymph/blood), is exceptional for its remarkable thinness, striking strength, and vast surface area. These properties formed to meet conflicting roles: thinness was essential for efficient flux of oxygen by passive diffusion, and strength was crucial for maintaining structural integrity. What we have designated as "three-ply" or "laminated tripartite" architecture of the barrier appeared very early in the evolution of the vertebrate gas exchanger. The design is conspicuous in the water-blood barrier of the fish gills through the lungs of air-breathing vertebrates, where the plan first appeared in lungfishes (Dipnoi) some 400 million years ago. The similarity of the structural design of the barrier in respiratory organs of animals that remarkably differ phylogenetically, behaviorally, and ecologically shows that the construction has been highly conserved both vertically and horizontally, i.e., along and across the evolutionary continuum. It is conceivable that the blueprint may have been the only practical construction that could simultaneously grant satisfactory strength and promote gas exchange. In view of the very narrow allometric range of the thickness of the blood-gas barrier in the lungs of different-sized vertebrate groups, the measurement has seemingly been optimized. There is convincing, though indirect, evidence that the extracellular matrix and particularly the type IV collagen in the lamina densa of the basement membrane is the main stress-bearing component of the blood-gas barrier. Under extreme conditions of operation and in some disease states, the barrier fails with serious consequences. The lamina densa which in many parts of the blood-gas barrier is <50 nm thin is a lifeline in the true sense of the word.

One approach to uncovering biological design principles is to ask what constraints they must obey. Apart from the laws of physics and chemistry, most constraints arise from evolution, which has selected particular solutions from a vast range of possible ones.

Hartwell et al. (92)

I. INTRODUCTION

From inexact assessments and deductions that suggested that the mean partial pressure of oxygen in the pulmonary capillary blood exceeded that in the alveolar gas, until fairly recently (91), it was presumed that, in the

lung, oxygen was actively absorbed (i.e., secreted) into the blood (see Ref. 67 for review and analysis of the historic debate). It is now certain that in all the evolved gas exchangers, be they water, air, or bimodal breathers, the flux of respiratory gases across the tissue barriers occurs entirely by passive diffusion along established partial pressure differences. In conformity with the physics of a passive process, the structural properties of a barrier influence the rate and efficiency of gas transfer. The diffusing capacity, or the conductance of a tissue barrier for oxygen, correlates directly with the surface area and inversely with the thickness of the partition (200).

Although compared with the closely located, visibly mechanically active heart, the lung may appear relatively inactive, for an organ that throughout life is subjected to changing internal and external pressures both by the pulsating heart and mechanical ventilation by the rhythmic contractions of the respiratory muscles, albeit passively, the lung is inherently a dynamic organ. Illustratively: in the human being, as much as 12,000 liters of air and 6,000 liters of blood per day are pumped into and through the lung (29); the lung is the only organ in the body across which the entire cardiac output and the systemic blood volume transits; of the total blood volume in the body, ~9% of it is contained in the lung (48), and pulmonary blood flow is pulsatile from the entrance of the pulmonary circulation to its outlet in the left atrium (126, 172), with the dampening of the pressure wave occurring in the blood capillary system (255).

Stemming from the physical properties of the respiratory medium utilized (air), lungs experience certain unique operational challenges: *1*) compared with the water-blood barrier of the fish gills that separates fluid media of equivalent specific densities (water and blood), the blood-gas barrier of the lung partitions air and blood, materials that are substantially different; consequently, in the lung, external physical support similar to that conferred to the gills by water is lacking and thus the blood-gas barrier is subjected to tensions emanating from the weight of its tissue, its blood, and the prevailing intramural blood pressures (249). *2*) While systemic blood vessels are physically anchored to the tissues in which they are located, pulmonary blood vessels are literally suspended in air by a diffuse fibroskeletal framework (237). States and factors such as the degree of inflation, perfusion pressure, surface tension, and hydrostatic pressure (56, 66, 118, 119, 224) determine the structure and organization of the connective tissue scaffold of the lung parenchyma.

The novel morphological states and physiological capacities that culminated in remarkable diversification and advancement of the modern animal life could not have happened without efficient respiratory organs. The question about why, when, and how the innovations arose, especially regarding the formation of a thin and extensive water/blood-gas barrier, is of particular interest to morphologists, physiologists, biophysicists, and evolutionary biologists in general. The challenges faced in evolving a structure of which the functional properties are totally at variance, thin to promote gas exchange and strong to tolerate tension, were formidable by any human engineering standards. (We have borrowed the word "design" from the engineers to describe the conception and assembly of what we have termed the three-ply or laminated tripartite architecture of the structural components that form the water/blood-gas barrier.)

While a complete understanding of the morphogenetic and molecular mechanisms by which the barrier was evolutionary fashioned is lacking, essentially comprising a thin epithelial cell that faces water/air, an extracellular matrix/interstitial space, and an endothelial cell that fronts the blood capillary, the three-ply design of the water/blood-gas barrier is highly conserved. Body designs that have changed little over the evolutionary continuum have been termed Bauplans (frozen cores) (227, 228). Such constructions are probably the only feasible and practical solutions to exacting functional requirements. The rarity of "fixed" designs in biology and their failure to evolve over hundreds of millions of years indicates nature's economy in establishing stable structures. It may connote the high cost of inaugurating and maintaining highly selected constructs. Discernment and study of the "defended" structural states are important for understanding the evolution of adaptive processes, i.e., the structural-functional correlations, and that of optimization in biology. The three-ply design of the water/blood-gas barrier has been in existence in the lungs of the lungfishes (Dipnoi) (108, 109, 128, 154), animals that have morphologically changed very little over their ~400 million years of evolution (10, 195, 220). Likely to have arisen from a common ancestral lineage with the stock that gave rise to the tetrapods, lungfishes are arguably reported to be the closest living relative to the tetrapods, i.e., amphibians, reptiles, birds, and mammals (27, 170, 258, 260, 261). Located at an important evolutionary crossroad, the dipnoans offer an informative model for gaining insights into the functional design of the vertebrate body.

The ultrastructural morphology and morphometry of the vertebrate gas exchangers, including that of the blood-gas barrier, have been described and reviewed severally: in mammals (41, 233, 234, 236–238), in birds (124, 142–144, 147, 148), in reptiles (125, 134, 161, 165–168, 186, 189–192, 194), in amphibians (43, 44, 45, 80–85, 131, 156, 166, 168), and in lungfishes (108, 128, 154). The water-blood barrier of the piscine gills has been extensively studied (105, 110). The capability of the water/blood-gas barrier to tolerate stress and its failure under extreme

conditions have, however, only been studied in the mammalian lung (reviewed in Refs. 247, 248, 250, 251).

This account comparatively examines the water/blood-gas barriers from the perspectives of their evolution and their structural and functional morphologies. It provides a comprehensive account of the compromise design that produced a functionally (mechanically) viable, thin tissue barrier that separates the respiratory fluid media in the gas exchangers. We have *1*) shown that the three-ply design of the water/blood-gas barrier is a shared structural feature of the gas exchangers that have evolved in the mainstream vertebrate taxa; *2*) debated and speculated on why, when, and how the barrier developed thinness while simultaneously preserving adequate strength for operation under conventional range of conditions; 3) taken into account that it has been inclusively exploited by diverse vertebrate taxa, the three-ply architecture of the water/blood-gas barrier has been conserved and perhaps optimized over its long period of evolution; *4*) presented credible, though indirect, evidence that the strength of the blood-gas barrier can largely be attributed to the presence of type IV collagen in the lamina densa of the extracellular matrix; and *5*) briefly discussed the extreme operational and pathological conditions and disease states under which the blood-gas barrier fails, with serious consequences. On account of scarcity and in certain cases, absolute lack of data on certain fundamental aspects of the evolution and morphogenesis of the blood-gas barrier (soft tissues like lungs are rarely, if ever, preserved by fossilization) and lack of extensive and meaningful molecular and genomic extrapolative studies (222), we are alert to the fact that certain deductions are presently conjectural. It is hoped that putative as they may be, such speculations will trigger further inquiry into an interesting area of biology.

II. DESIGN OF THE BLOOD-GAS BARRIER FOR GAS EXCHANGE

A. Flux of Oxygen Across the Blood-Gas Barrier: Biophysical Factors and Quantitative Considerations

No other molecular factor has had a singularly greater influence on the evolution and progress of animal life than oxygen (35, 86, 199). The advancement from the simple protozoan (unicellular) to the complex metazoan (multicellular) domains, transition from water breathing to air breathing, transformation from ectothermic-heterothermy to endothermic-homeothermy, and achievement of innovative locomotory capacities such as flight are but some of the consequential events that marked the change from low metabolic to highly aerobic states. Fluctuations in the levels of oxygen in the biosphere (86) set the cost and the efficiency of acquisition of molecular oxygen, fundamentally directing the nature and pace of evolutionary change.

On close scrutiny, one is impressed by the remarkable bioengineering challenges that were surmounted during the evolution of efficient, cost-effective respiratory structures and processes. Respiratory media (water/air and blood) had to be brought into close proximity and exposed to each other across an extensive, thin tissue barrier. To generate and maintain an adequate partial pressure gradient of oxygen (P_{O_2}), the respiratory fluid media had to be continuously moved and replenished. The tissue barrier had to withstand changing hemodynamic pressures from the blood capillary side, tolerate surface tension forces from the air fronting side, and encounter different physical, chemical, and biological insults. Over a lifetime, the barrier had to repair inevitable damages. Mechanical support had to be provided by well-placed connective tissue elements that did not intrusively compromise respiratory efficiency. Paradoxically, the refinements (i.e., thin and vast water/blood-gas barrier) that enhanced the respiratory efficiency inauspiciously conceded its effectiveness as a viable functional barrier and a meaningful physical deterrent of harmful inhaled microorganisms, allergens, carcinogens, toxic particles, and noxious gases. An assortment of lines of fortification was established to offset the contracted weaknesses/deficiencies. For example, a formidable selection of respiratory defenses that included airway secretions, cilia, respiratory reflexes (e.g., coughing), efficient lymphatic drainage, and surface (23, 24) and intravascular macrophages (147) were formed. Considering the many roles, including metabolic ones (7, 9, 64, 113), that the lung has acquired, the various structural requirements for optimal performance of the different roles have inevitably conflicted. Structural failure of the blood-gas barrier occurs under extreme states and conditions of operation.

Regarding the design of gas exchangers, structure relates to the form and organization of the constitutive parts that provide the means by which air and blood are brought into close proximity and exposed to each other while function appertains to mechanisms such as ventilation and perfusion, through which the respiratory fluid media are moved to maintain a high P_{O_2}. In the parenchyma of respiratory organs, blood capillaries anastomose profusely and in some cases protrude prominently into the respiratory spaces (see Fig. 2, *A–D*). The blood capillaries are virtually suspended in air (Fig. 1). The blood flow through the dense capillary network models a sheet (72, 141). Complex vascular architecture and delicate connective tissue network support the parenchyma (29, 234, 237, 239). For an oxygen flow (V_{O_2}) of 200 ml/min, only an average partial pressure difference of 0.057 kPa is needed for diffusion of oxygen across the blood-gas barrier, a process that occurs at a rate of 2.3×10^{-5} cm^2/s and is completed in 250–500 ms (88, 200, 246).

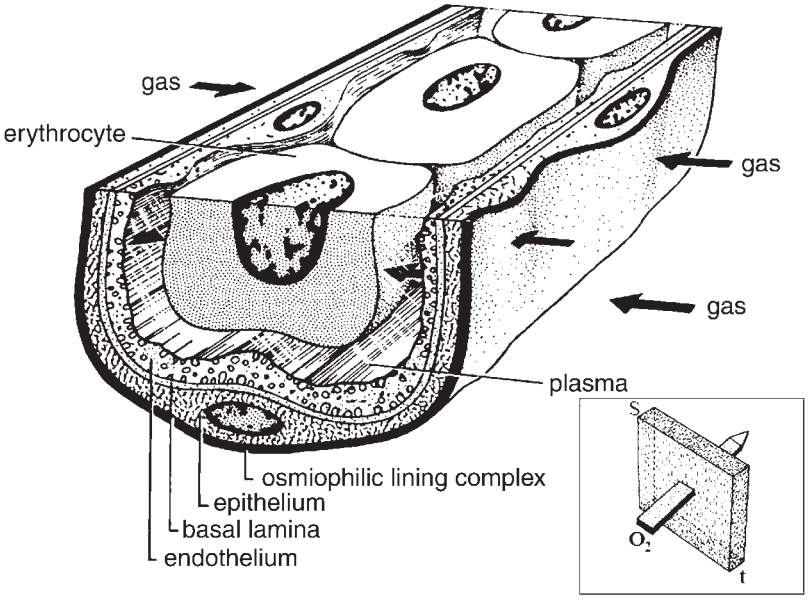

FIG. 1. Schematic diagram showing a cross-section of a pulmonary blood capillary containing red blood cells. Oxygen diffuses through the air-hemoglobin pathway that is comprised of the blood-gas barrier, a plasma layer, and red blood cell cytoplasm where it is chemically bound to hemoglobin. The diffusing capacity of a tissue barrier for oxygen correlates directly with surface area (s) and inversely with thickness (t) (*inset*). [From Maina (132).]

Given that gas exchangers transmit respiratory fluid media, water/air and blood through morphogenetically established conduits (bronchial airways and vascular channels) (33, 160) and diffusion of oxygen occurs across physical spaces en route to the mitochondrial furnaces, the designs of the respiratory organs invite mathematical analysis and modeling (19, 100, 132, 200, 230, 232, 240). Whilst generally considered a physiological parameter, the total morphometric diffusing capacity DL_{O_2} is greatly influenced by the structural attributes of the blood-gas barrier (i.e., surface area and thickness) and the pulmonary capillary blood volume (Figs. 2–4). Respiratory

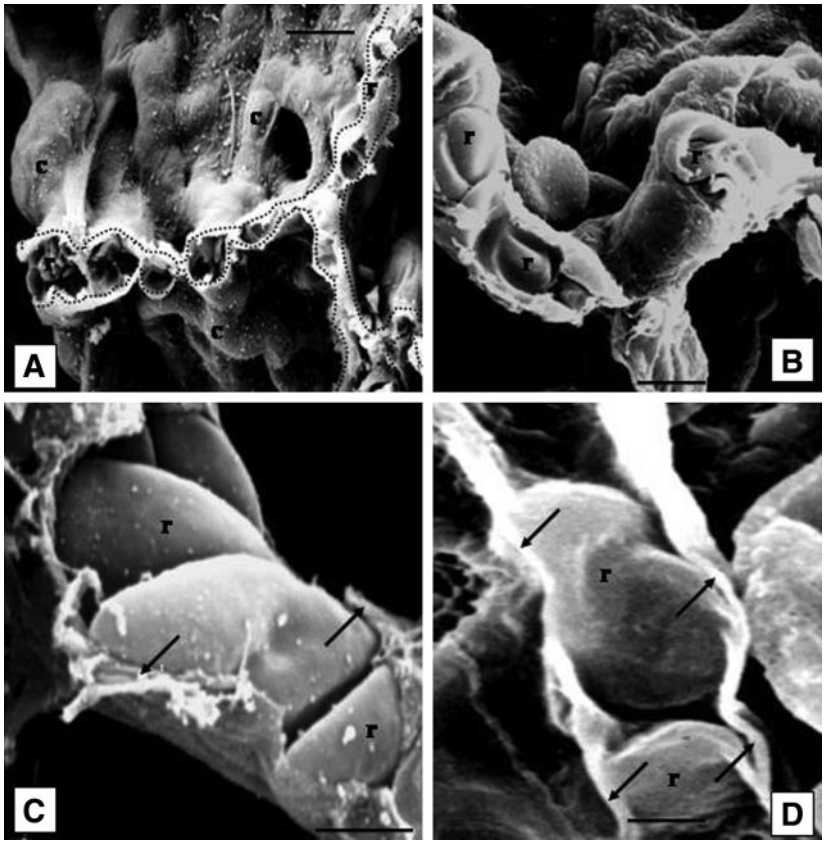

FIG. 2. *A*: interalveolar septum (dashed lines) of the lung of the bushbaby, *Galago senegalensis*. c, Blood capillaries; r, red blood cells. Scale bar is 25 μm. [From Maina (142).] *B*: interalveolar septum of the lung of a vervet monkey, *Cercopithecus aethiops*, showing blood capillaries containing red blood cells (r). Scale bar is 15 μm. [From Maina (130a).] *C*: a blood capillary in the exchange tissue of the lung of the domestic fowl, *Gallus domesticus*, showing red blood cells (r) and blood-gas barrier separating blood from air (arrows). Scale bar is 5 μm. [From Maina (138a).] *D*: a blood capillary in the lung of a bat, *Epomophorus wahlbergi*, showing blood-gas barrier (arrow) separating air and blood. r, Red blood cells. Scale bar is 8 μm.

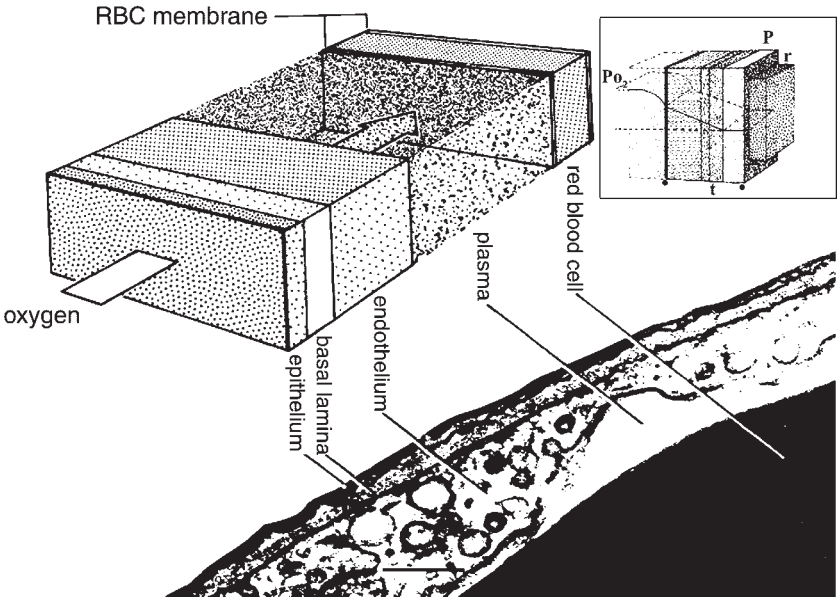

FIG. 3. A schematic diagram and an electron micrograph showing the barriers through which oxygen diffuses. These are the tissue barrier that is comprised of an epithelial cell, extracellular matrix, and an endothelial cell, plasma layer, and red blood cell (RBC) cytoplasm. The Po_2 decreases with the diffusional distance (*inset*), i.e., as oxygen passes through the tissue barrier (t), plasma layer (p), and the red blood cell cytoplasm (t). Scale bar is 0.3 μm. [From Maina (142).]

physiologists recognized this fact very early. Roughton and Forster (200) separated DLo_2 into "membrane diffusing capacity, Dmo_2," i.e., the flow of oxygen through the blood-gas barrier, and that of the "blood components, Deo_2," the rate at which oxygen binds to the hemoglobin.

With the use of relevant morphometric measurements (Figs. 1 and 3) and the physicochemical coefficients of permeation of oxygen through the various components, the diffusing capacities of the different parts of the air-hemoglobin pathway and the total (overall) value for the lung (DLo_2) can be estimated (132, 153, 232, 240). According to Fick's first law of diffusion, oxygen flow rate across a tissue barrier is directly proportional to the cross-sectional surface area (*S*) and inversely proportional to the thickness of the barrier separating the respi-

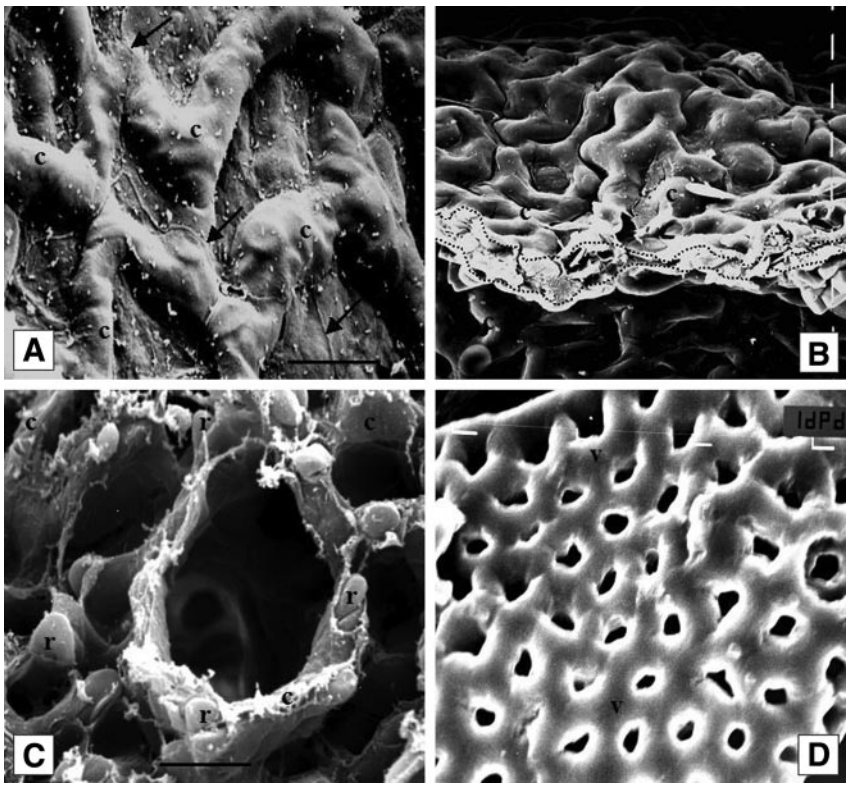

FIG. 4. *A*: alveolar surface of the lung of the bushbaby, *Galago senegalensis*. Type I cells (arrows) that are thin and expansive cover respiratory surface. Blood capillaries (c) protrude into the alveolar space. Scale bar is 20 μm. [From Maina (141).] *B*: lung of a snake, the black mamba, *Dendroaspis polylepis*, showing blood capillaries anastomosing and protruding into the adjacent air space. Dashed lines delineate the interfaveolar septum. Scale bar is 50 μm. *C*: lung of the domestic fowl, *Gallus domesticus*, showing air capillaries surrounded by blood capillaries (c) that contain red blood cells (r). Scale bar is 10 μm. *D*: surface of a secondary lamella of the gills of a teleost fish, *Alcolapia grahami*, showing profuse vascular channels (v) that are separated by pillar cells. Scale bar is 20 μm. [From Maina (141).]

ratory media (Figs. 1 and 2, *insets*). Oxygen flow (V_{O_2}) is determined by the P_{O_2} and the permeability coefficient (K) [i.e., the product of solubility and diffusion coefficients (α) and (D), respectively] through the components of the barrier. Thus

$$V_{O_2} = K \cdot S \cdot \tau^{-1} \cdot \Delta P_{O_2} \quad (1)$$

Fick's law is analogous to Fourier's law of heat conduction in physics; heat flow (Q) is given by the relation

$$Q = kA \cdot [T_1 - T_2] \cdot l^{-1} \quad (2)$$

where A is the cross-sectional surface area, l is the distance between the two ends of the conducting material, T_1 and T_2 are the difference in temperature between the two ends of the conductor, and k is the proportionality constant (called the thermal conductivity) specific to the material properties of the conductor.

The total distance traversed by an oxygen molecule (here called the "air-hemoglobin pathway") includes the blood-gas (tissue) barrier, the plasma layer (space between the endothelial cell and the cell membrane of the erythrocyte), and the erythrocyte cytoplasm, i.e., the distance that an oxygen molecule travels before it is chemically bound to hemoglobin (Figs. 2 and 3). The components of the air-hemoglobin pathway are arranged in series (Fig. 3), i.e., an oxygen molecule sequentially passes through the structural components. The total resistance that the molecule encounters (R_o) is thus the sum of the individual resistances, i.e., those of the blood-gas barrier (t), the plasma layer (p), and the erythrocyte (e). Thus

$$R_o = R_t + R_p + R_e \quad (3)$$

With the reciprocal of resistance being the conductance (i.e., the diffusing capacity), the DL_{O_2} is in turn the sum of the reciprocals of the conductances of the components of the air-hemoglobin pathway, namely, the diffusing capacity of the tissue barrier (Dt_{O_2}), that of the plasma layer (Dp_{O_2}), and that of the erythrocyte (De_{O_2}). Thus

$$1/DL_{O_2} = 1/Dt_{O_2} + 1/Dp_{O_2} + 1/De_{O_2} \quad (4)$$

The total morphometric pulmonary diffusing capacity for oxygen (DL_{O_2}) offers an estimate of a gas exchanger capacity of transferring oxygen under ideal conditions, i.e., where inequalities of ventilation and perfusion are nonexistent and the entire blood-gas barrier is involved in the transfer oxygen. The parameter is meaningful in assessing and comparing gas exchange potentials of different respiratory organs.

Pathological and adaptive changes may occur in any of the components of the air-hemoglobin pathway. For example, edema increases the thickness of the blood-gas (tissue) barrier, dehydration may reduce the thickness of the plasma layer, and anemia may affect the oxygen binding characteristics of the hemoglobin. For example, while diving birds like penguins have relatively thick blood-gas barriers (129, 245), a feature alleged to forestall collapse of the air capillaries under hydrostatic pressures during dives (245), such birds have particularly large pulmonary capillary blood volumes (V_c) (129, 132, 150, 153). The large V_c gives a high De_{O_2} that in turn offsets the limitations caused by a thick tissue barrier (reflected in a low Dt_{O_2}). In the Humboldt penguin, *Spheniscus humboldti* (150), and in the emperor penguin, *Aptenodytes forsteri* (245), with values of 0.53 and 0.66 μm, respectively, the harmonic mean thicknesses of the blood-gas barrier (τ_{ht}) are exceptionally thick (Table 1); while Dt_{O_2} itself is low, the high De_{O_2} raises DL_{O_2} to match that of nondiving (flying) birds of equivalent body mass (144, 150).

An important caveat to remember in respiratory functional morphology (morphometry) is that analyzing structural components and making inferences based on individual measurements may potentially lead to erroneous conclusions regarding adaptive biologies, e.g., the efficiencies of different gas exchangers. This is because the constitutive components work as an integrated system and not individually. Moreover, certain trade-offs and compromises may be involved in the formation of their ultimate morphologies and morphometries. Notwithstanding the existing limitations, especially those relating to lack of physical coefficients of the binding of oxygen to hemoglobin and the permeation of oxygen through the structural components of the air-hemoglobin pathway in the gas exchangers of many species, pulmonary modeling is highly desirable.

B. Comparative Observations on the Structure of the Blood-Gas Barrier

In gas exchangers, the barrier across which molecular oxygen diffuses from an external respiratory medium (water/air) to blood is comprised of a motley crew of cellular elements and a suite of supporting structural components. Various epithelial cells (pneumocytes) line the surface; the extracellular matrix or interstitium contains sparsely scattered connective tissue elements like collagen, elastic tissue, and smooth muscle; while an endothelial cell lines the blood capillaries. Evidently a product of a bioengineering blueprint that utilizes minimal structural materials, the remarkably thin blood-gas barrier allows efficient exchange of respiratory gases by passive diffusion. In the particularly thin regions of the interalveolar septum of the mammalian lung (143) and between the air and blood capillaries of the avian lung, the barrier is pretty much formed by squamous (thin),

TABLE 1. *Harmonic (τ_{ht}) and arithmetic (τ_t) mean thicknesses of the blood-gas (tissue) barrier, harmonic mean thickness of the plasma layer (τ_{hp}), and minimum harmonic mean thickness of the blood-gas (tissue) barrier [τ_{ht} (min)] in lungs of various vertebrate taxa*

Order/Species	Body Mass, kg	τ_{ht}, μm	τ_{ht} (min), μm	τ_{hp}, μm	τ_t, μm	τ_t/τ_{ht}
			Birds			
Struthioformes						
Ostrich[a]	45	0.560		0.140	0.690	1.23
Struthio camelus						
Sphenisciformes						
Humboldti penguin[b]	4.5	0.530		0.213		
Spheniscus humboldti						
Anseriformes						
Mallard duck[c,d,e]	1.04	0.113	0.062	0.369	0.903	6.80
Anas platyrhynchos						
Greylag goose[c,d,e]	3.84	0.118	0.050	0.322	0.887	7.85
Anser anser						
Muscovy duck (domestic)[f]	1.63	0.199	0.051	0.337	0.303	1.52
Carina moschata						
Falconiformes						
Common kestrel[c,d]	0.066	0.210	0.099	0.252	1.662	7.91
Falco tinnunculus						
Galliformes						
Domestic fowl[g]	2.141	0.318		0.306	1.24	3.90
Gallus gallus (domestic)						
Guinea fowl (domestic)[h]	1.839	0.320			1.12	3.50
Numida meleagris (domestic)						
Domestic turkey[i]		0.385	0.177		0.637	1.65
Meleagris gallopavo (domestic)						
Gruiformes						
White-breasted water hen[f,g]	0.146	0.204	0.099	0.384	0.395	1.94
Amaurornis phoenicurus						
Charadriiformes						
Razorbill[c,d,j]	0.487	0.230		0.254	0.803	3.49
Alaca torda						
Spectacled guillemont[c,d,j]	0.737	0.193		0.280	0.850	4.40
Cephus carbo						
Herring gull[c,d,j]	0.654	0.153	0.075	0.399	1.27	8.33
Larus argentatus						
Common gull[c,d,j]	0.302	0.116		0.272	0.684	5.90
Larus canus						
Black-headed gull[c,d,j]	0.253	0.146	0.071	0.306	0.925	6.34
Larus ridibundus						
Columbiformes						
Rock dove[c,d]	0.216	0.161		0.197	0.804	4.99
Columba livia (domestic)						
Collared turtle dove[c,d]	0.189	0.218		0.160	0.801	3.67
Streptopelia decaocta						
Laughing gull[c,d]	0.058	0.227		0.166	0.986	4.34
Streptopelia senegalensis						
Pstitaciformes						
Budgerigar[c,d,i]	0.04 ± 0.001	0.12 ± 0.001	0.07 ± 0.001	0.14 ± 0.17	0.59 ± 0.54	5.06 ± 4.63
Melopsitacus undulatus						
Cuculiformes						
Klaa's cuckoo[c,d]	0.027	0.157		0.236	0.679	0.433
Chrysococcyx klaas						
Apodiformes						
Violet-eared hummingbird[i]		0.099	0.062	0.017	0.183	1.85
Colibri coruscans						
Coliiformes						
Spectacled mousebird[c,d]	0.050	0.148		0.265	0.761	5.14
Colius striatus						
Piciformes						
Golden-rumped tinkerbird[c,d]	0.015	0.165		0.191	1.01	6.12
Pogoniulus bilineatus						
Casuariiformes						
Emu[l]	30.0	0.232		0.103		
Dromaius novaehollandiae						
Passeriformes						
Grosbeak weaver[c,d,k]	0.037	0.121		0.201	0.584	4.83
Ambryospiza albifrons						
Singing cisticola[c,d,k]	0.015	0.122		0.219	0.608	4.98
Cisticola cantans						
African rock martin[c,d,k,l]	0.014	0.090		0.172	0.613	6.81
Hirundo fuligula						
Fiscal shrike[c,d,k]	0.033	0.170		0.216	0.638	3.75
Lanius collaris						

TABLE 1—*Continued*

Order/Species	Body Mass, kg	τ_{ht}, μm	τ_{ht} (min), μm	τ_{hp}, μm	τ_t, μm	τ_t/τ_{ht}
House sparrow[c,d,k] *Passer domesticus*	0.026	0.096	0.052	0.217	1.03	10.77
Baglafecht weaver[c,d,k] *Ploceus baglafecht*	0.033	0.151		0.215	0.762	5.05
Twany prinia[c,d,k] *Prinia subflava*	0.009	0.124		0.197	0.675	5.44
Common stirling[c,d,k] *Sturnus vulgaris*	0.073	0.141	0.065	0.226	1.124	7.87
Redwing[c,d,k] *Turdus iliacus*	0.051	0.120	0.060	0.457	1.012	8.43
Olive thrush[c,d,k] *Turdus olivaceus*	0.065	0.127		0.234	0.599	4.72
		Mammals				
Domestc pig[m]		0.72	0.19		1.90	2.64
Sheep[m]		0.68	0.20		1.87	2.75
Rhesus monkey[m]		0.65	0.19		1.80	2.77
Rabbit[m,n] *Oryctolagus cuniculus*		0.58 ± 0.11	0.24	0.180	1.40	2.15
Hamster[m]		0.56	0.19		1.49	2.66
Gerbil[m]		0.51	0.20		1.34	2.63
Mouse[m]		0.44	0.19		1.27	2.89
Olive baboon[o] *Papio anubis*	18.85	0.478		0.203	1.12	2.34
Lesser bushbaby[p] *Galago senegalensis*	1.12	0.355		0.174		
Shrews[n]	0.02 ± 0.03	0.34 ± 0.05		0.11 ± 0.02		
White rat[n] *Rattus rattus*	0.140	0.385				
Japanese waltzing mouse[n] *Mus wagneri*	0.013	0.256		0.126		
Suni[n] *Nesotragus moschatus*	3.3	0.562		0.182		
Genet cat[n] *Genetta tigrina*	1.37	0.485		0.117		
Dik dik[n] *Madoqua kirkii*	4.2	0.446		0.187		
Monkey[n] *Macaca irus*	3.71	0.50		0.180		
Banded mongoose[n] *Mungos mungo*	1.14	0.409		0.181		
Dwarf mongoose[n] *Helogale pervula*	0.53	0.394		0.167		
Guinea pig[n] *Cavia porcellus*	0.429	0.42		0.187		
White mouse[n] *Mus musculus*	0.042	0.32		0.143		
Camel[n] *Camelus dromedarus*	231.7	0.60				
Giraffe[n] *Giraffa camelopardalis*	383	0.60				
Dog[m,n] *Canis familiaris*	23.4 ± 17.8	0.52 ± 0.1	0.22		1.78	1.11
Wildebeest[n] *Connochaetes taurinus*	102.0	0.37				
Waterbuck[n] *Kobus defassa*	109.8	0.46				
African goat[n] *Capra hircus*	20.9	0.54				
African sheep[n] *Ovis aries*	21.8	0.53				
Swiss cow[n] *Bos taurus*	700.0	0.51				
Horse[n] *Equus caballus*	510.0	0.60				
Zebu cattle[n] *Bos inducus*	192.5	0.50				
Eland[n] *Taurotragus oryx*	240.0	0.50				
Human *Homo sapiens*	74.0	0.62				
Thompson's gazelle[n] *Gazella thompsani*	19.5	0.37				
Naked mole rat[q] *Heterocephalus glaber*	0.031	0.243		0.210	1.091	4.49

TABLE 1—*Continued*

Order/Species	Body Mass, kg	τ_{ht}, μm	τ_{ht} (min), μm	τ_{hp}, μm	τ_t, μm	τ_t/τ_{ht}
Ground mole rat[q] *Tachyoryctes splendens*		0.203		0.219	0.678	3.34
Grant's gazelle[n] *Gazella granti*	10.1	0.54				
Bats[r]	0.25 ± 0.32	0.30 ± 0.01		0.14 ± 0.05	1.39 ± 0.11	6.04 ± 0.78
			Reptiles			
Green lizard[m] *Laceta viridis*		0.90	0.24		1.96	2.18
Wall lizard[m] *Lacerta muralis*		0.84	0.21		1.69	2.01
Garden lizard[m] *Calotes nemoricola*		1.03	0.25		1.99	1.93
Blind-slow worm[m] *Anguis fragilis*		0.90	0.20		2.06	2.29
European chameleon[m] *Chamaeleo chamaeleon*		0.73	0.18		1.68	2.30
Grass snake[m] *Natrix natrix*		1.34	0.20		2.42	1.81
Smooth snake[m] *Coronella austriaca*		1.02	0.25		2.31	2.26
American alligator[m] *Alligator mississippiensis*		0.73	0.20		1.65	2.26
European tortoise[m] *Testudo graeca*		1.38	0.23		2.49	1.80
Red-eared turtle[m] *Pseudemys scripta*		1.19	0.23		2.10	1.76
Teju[s] *Tupinambis nigropunctatus*		0.46				
Lacerta[t] *Varanus exanthamaticus*		0.53				
Snake[u] *Pituophis melanoleucus*		0.46				
Turtle[v] *Pseudemvs scripta*		0.50				
Crocodile[w] *Crocodylus niloticus*		1.4				
Tokay[x] *Gekko gecko*		1.08				
			Amphibians			
South African clawed toad[m] *Xenopus laevis*		1.21	0.24		1.71	1.41
Nigerian clawed toad[m] *Xenopus tropicalis*		1.23	0.19		1.75	1.42
Common frog[m] *Rana temporaria*		1.50	0.21		2.06	1.37
Bull frog[m] *Rana catesbeiana*		1.72	0.20		1.95	1.13
Northern leopard frog[m] *Rana pipiens*		1.53	0.20		2.04	1.33
Common toad[m] *Bufo bufo*		1.67	0.19		1.85	1.11
European spotted salamander[m] *Salamandra salamandra*		1.78	0.25		2.30	1.29
Fire-bellied newt[m] *Paramesotriton hongkongensis*		1.81	0.19		2.60	1.44
Common newt[m] *Triturus vulgaris*		2.34	0.25		2.63	1.12
Italian crested newt[m] *Triturus cristatus*		2.20	0.20		2.81	1.28

Sources of data: [a] Maina and Nathaniel (158); [b] Maina and King (150); [c] Maina (132); [d] Maina et al. (153); [e] Maina and King (148); [f] Vidyadaran et al. (226); [g] Abdalla et al. (2); [h] Abdalla and Maina (1); [i] Dubach (51); [j] Maina (128); [k] Maina (127); [l] Maina and King (151); [m] Meban (168); [n] Gehr et al. (75); [o] Maina (130); [p] Maina (137); [q] Maina et al. (157); [r] Maina and King (149); [s] Perry (189); [t] Cragg (38); [u] Stinner (213); [v] Perry (188); [w] Perry (191); [x] Perry et al. (193).

parallel cytoplasmic extensions of the epithelial (type 1) and endothelial cells that are literally "glued" back to back, onto an extracellular matrix (Figs. 5 and 6). The architecture has been described as a three-ply or laminated tripartite design.

1. The water-blood barrier of the fish gills

Gills are the archetypal water breathing organs (99, 105, 140). Those of teleosts are structurally the most complex. Commonly, four gill (branchial) arches give rise

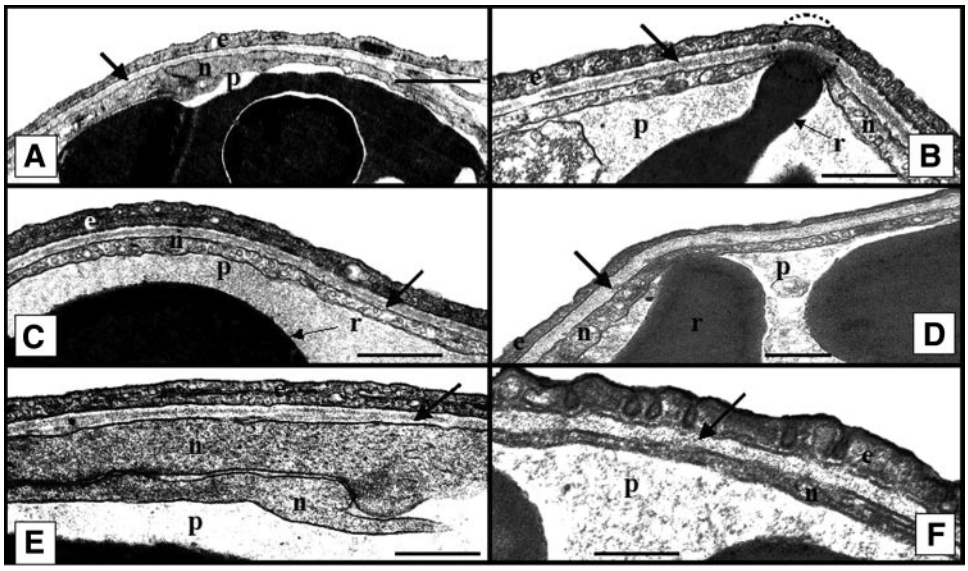

FIG. 5. *A*: blood-gas barrier of the lung of the African lungfish, *Protopterus aethiopicus*, showing epithelial cell (e) extracellular matrix (arrow), endothelial cell (n), and plasma layer (p). Scale bar is 4 μm. *B*: blood-gas (tissue) barrier of the lung of a tree frog, *Chiromantis petersi*, showing an epithelial cell (e) extracellular matrix (arrow), endothelial cell (n), plasma layer (p), and red blood cell (r). Dashed circle represents the area where a red blood cell is pressing onto the tissue barrier. Scale bar is 3 μm. [From Maina (140a).] *C*: blood-gas (tissue) barrier of the lung of the pancake tortoise, *Malacochersus tornieri*, showing an epithelial cell (e) overlying extracellular matrix (arrow), endothelial cell (n), plasma layer (p), and red blood cell (r). Scale bar is 5 μm. *D*: blood-gas (tissue) barrier of the lung of the monitor lizard, *Varanus exanthematicus*, showing an epithelial cell (e), extracellular matrix (arrow), endothelial cell (n), plasma layer (p), and red blood cell (r). Scale bar is 5 μm. *E*: blood-gas (tissue) barrier of the lung of a snake, the black mamba, *Dendroaspis polylepis*, showing an epithelial cell (e), extracellular matrix (arrow), fusing endothelial cells (n), and plasma layer (p). Scale bar is 2 μm. [From Maina (134).] *F*: blood-gas (tissue) barrier of the lung of a snake, the sandboa, *Eryx colubrinus*, showing an epithelial cell (e), extracellular matrix (arrow), an endothelial cell (n), and plasma layer (p). Scale bar is 3 μm.

to hundreds of gill filaments that in turn originate thousands of secondary lamellae (Fig. 7, *A* and *B*). The hierarchical arrangement produces extensive respiratory surface area in the confined space under the opercular flap, without invoking undue resistance to water flow (100). In some species of fish, e.g., *Barbus sophor*, secondary lamellae give rise to tertiary lamellae (106). The secondary lamellae are semicircular flaps that are bilaterally located on gill filaments (Fig. 7, *A–C*); they are the functional (respiratory) units of the teleost gills. The lamellae are comprised of two parallel sheets of epithelial cells that are connected by pillar cells that are highly characteristic of the ultrastructure of the teleost gills (110) (Figs. 4*D* and 7, *B*, *D*, and *E*). Containing abundant intracytoplasmic microfibrillar elements (13, 104, 209), the cells are contractile. The pillar cells maintain the mechanical integrity of the vascular channels, where blood pressure may reach 90 mmHg (12 kPa) (13, 101), and regulate lamellar perfu-

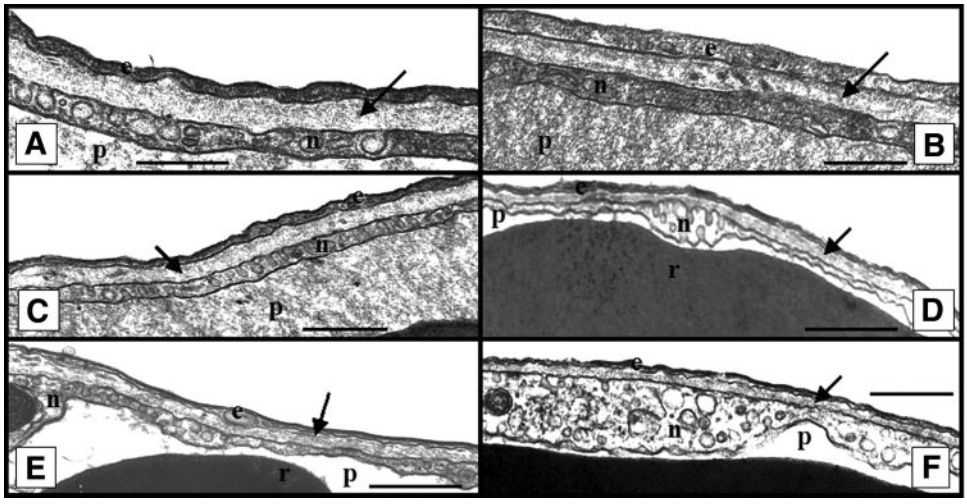

FIG. 6. *A–C*: blood-gas barrier of the mammalian lung from, respectively, a bushbaby, *Galago senegalensis;* the naked mole rat, *Heterocephalus glaber*; and a bat, *Miniopterus minor*. e, Epithelial cell; arrow, extracellular matrix; n, endothelial cell; p, plasma layer. Scale bars are as follows: *A*, 3 μm; *B*, 3 μm; *C*, 2 μm. *D–F*: blood-gas (tissue) barrier of the avian lung from, respectively, the house sparrow, *Passer domesticus*; the emu, *Dromaius novaehollandiae;* and the black-headed gull, *Larus ridibundus*. e, Epithelial cell; arrow, extracellular matrix; n, endothelial cell; p, plasma layer; r red blood cell. Scale bars are as follows: *D*, 0.4 μm; *E*, 0.5 μm; *F*, 0.3 μm. [*F* from Maina (132).]

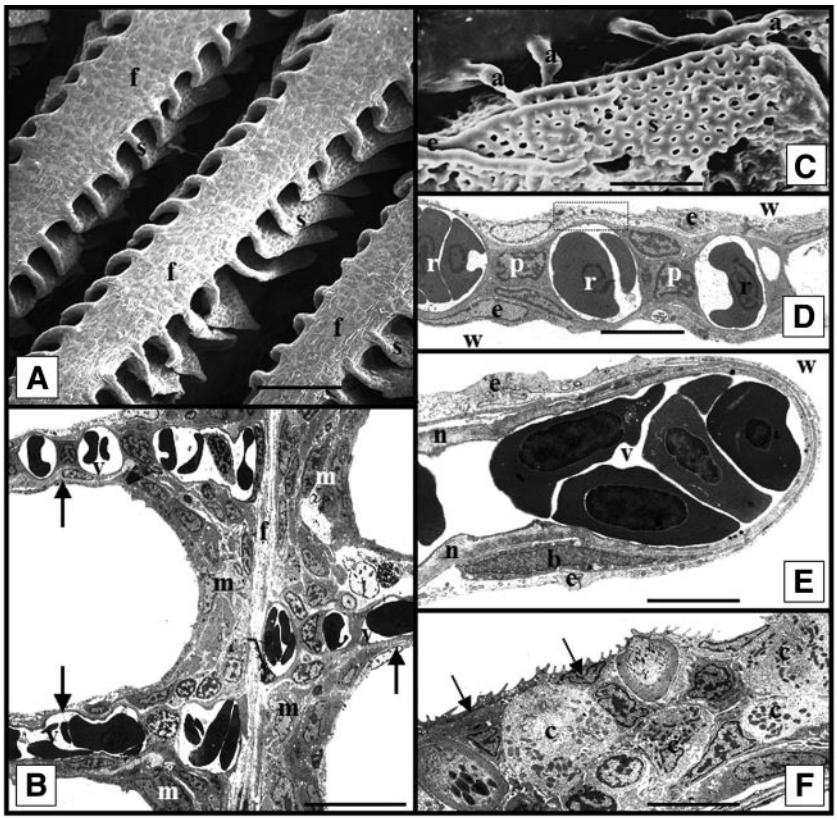

FIG. 7. *A*: gills of a teleost fish, *Alcolapia grahami*, showing gill filaments (f) and secondary lamellae (s). Scale bar is 1 mm. [From Maina (140a).] *B*: a gill filament (f) giving rise to secondary lamellae (arrows) that contain vascular channels (v). m, Primary epithelium. Scale bar is 0.5 mm. [From Maina (142).] *C*: a secondary lamella (s) receiving blood from a gill filament artery through afferent vessels (a). e, Efferent lamella blood vessel. Scale bar is 0.20 mm. [From Maina (141).] *D*: a secondary lamella showing vascular channels containing red blood cells (r). w, Water; e, epithelial cells; p, pillar cells; dashed area, water-blood barrier. Scale bar is 40 μm. [From Maina (141).] *E*: a marginal channel (v) of a gill filament. w, Water; e, epithelial cells; n, endothelial cells; b, interstitial cell. Scale bar is 15 μm. *F*: the composite primary epithelium of a gill filament showing pavement (epithelial) cells (arrows) and numerous chloride cells (c). Scale bar is 30 μm.

sion. The cytoplasmic flanges of the pillar cells form the innermost (endothelial) component of the water-blood barrier (110, 173) (Fig. 7, *B*, *D*, and *E*). An interstitial space that contains connective tissue and cellular elements as well as lymphatic vessels occurs between the endothelial cells and the epithelial cells (100) (Fig. 7, *D* and *E*). Although the structure of the water-blood barrier in the fish gills differs in certain aspects from the blood-gas barrier of the vertebrate lung, a three-ply design is positively perceptible (Fig. 7, *B*, *D*, and *E*). The architecture is evident from the gills of the archaic coelacanth *Latimeria chalumnae* species (102, 103) to the modern teleost species (105); the design has been conserved for a long time in diverse species of fish.

Gill epithelial lining is divided into respiratory and metabolic sites (30, 198). The complex vascular anatomy of the gills (73, 169, 180) is thought to be fundamental to the adjustment of the respiratory and osmoregulatory surface areas. Gas exchange largely occurs across the simple, thin secondary epithelium that covers the secondary lamellae (Fig. 7, *B*, *D*, and *E*), while metabolic functions, e.g., osmoregulation and ammonia/urea excretion, occur in the more elaborate primary epithelium that lines the gill filaments (121, 136). Chloride (mitochondria-rich) and mucus cells occur in the primary epithelium (Fig. 7*F*). Adjustment of the functional sites on fish gills optimizes respiratory and metabolic performances; a fish at rest maintains a small respiratory surface area to procure the needed amount of oxygen for its metabolizing tissues to remain aerobic without risking excessive loss or overloading of ions.

2. Relationship between three-ply (laminated, tripartite design) and evolution of open circulation

Occurring in, e.g., annelids cephalopods and vertebrates, while lacking in arthropods and most mollusks, closed circulation (where a continuous endothelial lining delimits the vascular conduits), can (from ontogenetic perspective) be associated with the formation of the three-ply design in the gas exchangers (32, 105). The transition from open to closed circulation is but one of the many quantum leaps that occurred in the process of the evolution and refinement of the respiratory organs and processes (139–141). In addition to occurring in the mainstream gas exchangers, i.e., gills and lungs, the three-ply design is manifest in the accessory respiratory organs such as the suprabranchial chamber membrane and the labyrinthine organs of bimodal breathing fish (107, 155) (Fig. 8, *A* and *B*), structures that develop from the gills (107). The air-blood barrier in the physostomatous swim bladders of fish, organs that are commonly used as accessory respiratory organs (162), presents a three-ply design (Fig. 8, *C* and *D*).

In the invertebrate animals with an open circulation, three-ply design is lacking in the respiratory organs. In the lung of the tropical terrestrial slug, *Trichotoxon copleyi* (133), epithelial cells attach onto basement membrane

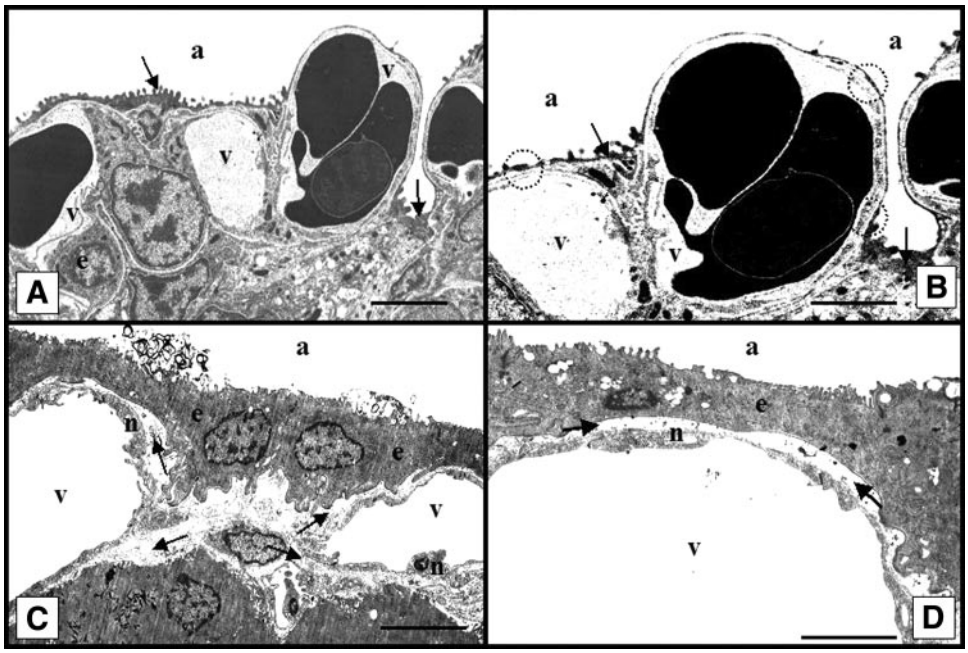

FIG. 8. *A*: surface of the suprabranchial chamber membrane of the catfish, *Clarias mossambicus*, showing epithelial cells (arrows), vascular channels (v) containing red blood cells (r), and endothelial cell (e). Scale bar is 30 μm. *B*: close-up of surface vasculature of the suprabranchial chamber membrane of the catfish, *Clarias mossambicus*, showing a visibly laminated tripartite blood-gas barrier particularly in sites shown by dashed circles. Arrows, epithelial cells; v, vascular channels; a, air space. Scale bar is 15 μm. *C* and *D*: blood vessels (v) on the surface of the physostomous swim bladder of a fish, *Alcolapia grahami*. a, Air space; e, epithelial cell; arrows, extracellular matrix; n, endothelial cell. Scale bars are as follows: *C*, 15 μm; *D*, 8 μm.

while an endothelial lining of the vascular channels is lacking (Fig. 9, *A* and *B*). The hemolymph comes into direct contact with the epithelial cells. In the gill filaments of the freshwater African crab, *Potamon niloticus* (135) (Fig. 9, *C* and *D*), the vascular channels are exclusively formed by epithelial cells (Fig. 9*D*). The cells attach onto a basement membrane that fronts the external respiratory medium (water) while the apical aspect faces the hemolymphatic channel. The low blood pressure in open circulatory systems may allow the formation of less complex and conceivably potentially weaker water/air-blood barriers. With a better constructed tissue barrier, closed circulation permitted higher blood pressure, shorter circulatory time, and more efficient perfusion of the body tissues, features that were vital for the greater metabolism in the more advanced animals (197).

3. Cellular and connective tissue elements of the blood-gas barrier

Together with the blood cells, the mammalian lung is reported to have an assortment of more than 40 different

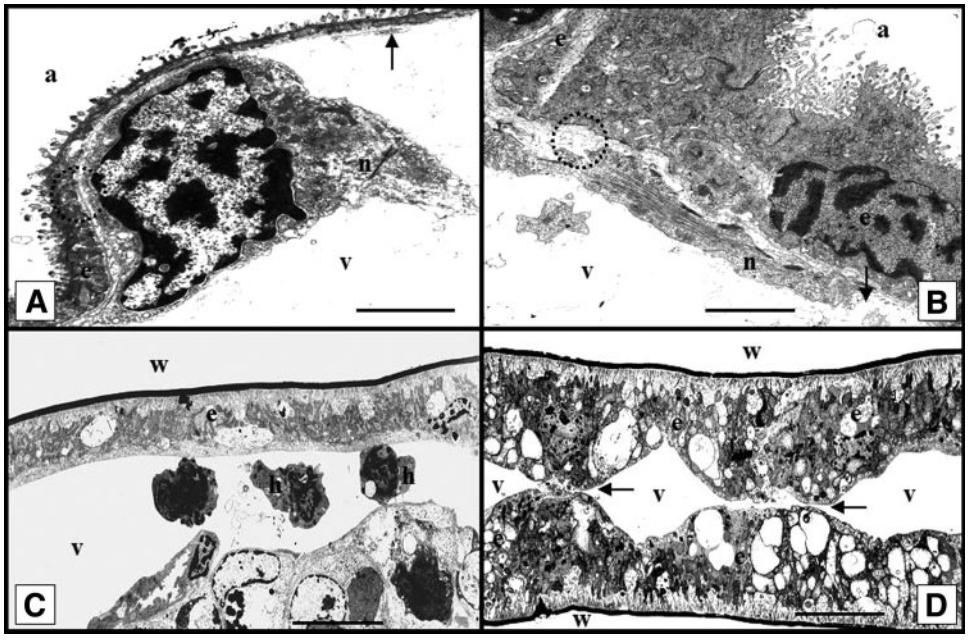

FIG. 9. *A*: lung of a slug, *Trichotoxon copleyi*, showing an endothelial cell (n) protruding into a hemolymphatic vessel. Dashed circle represents the area where an epithelial cell (e) lies next to an endothelial cell. Arrow, discontinuous endothelial cell lining; a, air space. Scale bar is 5 μm. [From Maina (133).] *B*: lung of a slug, *Trichotoxon copleyi*, showing epithelial cells (e) overlying extracellular matrix. Arrow and dashed circle show a thinned or discontinuous endothelial cell (n). v, Vascular channel. Scale bar is 20 μm. [From Maina (133).] *C*: hemolymphatic vessel (v) in a gill filament of a freshwater crab, *Potamon niloticus*, showing hemocytes (h). w, Water; e, epithelial cell. Scale bar is 50 μm. [From Maina (140b).] *D*: hemolymphatic channels (v) in a gill filament of the freshwater crab, *Potamon niloticus*, showing epithelial cells (e) meeting at regular intervals (arrows) to separate the channels. Scale bar is 30 μm. [From Maina (135).]

cell types (4, 25, 235). Less than 20 of them occur at the alveolar level (29) where the type 1 and type 2 cells are the major ones. With an average volume of 1,500 μm^3 and covering a mean surface area of 5,000 μm^2 (39, 40), the type 1 cells (squamous pneumocytes) have long extremely thin cytoplasmic extensions (Figs. 4*A*, 5, 6, and 10, *A* and *D*) that stretch over a distance of ~50 μm from the cell body (perikaryon). The trilaminar substance in the cytoplasm of the type 1 cells of the avian lung is thought to constitute an intercapillary "skeletal" support system (117). While constituting only ~10% of the total cell population, the type 1 cells cover as much as 96% of the alveolar surface (40). The type 2 cells (granular pneumocytes) are cuboidal in shape (Fig. 10*B*). Of an average volume of 550 μm^3 and constituting ~12% of the total cell population, the type 2 cells cover only ~5% of the alveolar surface. Compared with the type 1 cells that are largely devoid of organelles, the type 2 cells are secretory. They are well endowed with organelles and have characteristic microvilli on their free surface (Fig. 10*B*). The type 2 cells secrete the surfactant, material that contains dipalmitoylphosphatidylcholine, a surface-active phospholipid substance that stabilizes the alveoli (36, 46, 78, 163, 187). Osmiophilic lamellated bodies, organelles that are characteristic to the type 2 cells, are the precursors of the surfactant (Fig. 10*B*). Interestingly, akin to the three-ply design of the water/blood-barrier, the immunochemical proximity of the constitutive protein components of the surfactant has been highly and widely conserved (196). Among vertebrates, the surfactant is believed to have a single evolutionary origin (181, 215). Although particularly well-known in the vertebrate lung, to varying extents, the surfactant occurs in a range of organs, e.g., the intestinal mucosae and the swimbladder of actinopterygian fish, mesothelial tissues (mesentery, peritoneum, and pleura), synovial cells, Eustachian tubes, and probably in the salivary glands, pancreas, and urinary tract (20). Type 3 (brush) cells occur rarely in the vertebrate lung (49, 84, 171). The cells are typically pyramidal in shape, their free surface has large blunted microvilli, the cytoplasm contains numerous glycogen granules, and abundant intracytoplasmic microfilaments form a cytoskeletal system. Type 3 cells have been associated with functions like chemoreception, absorption, and secretion (49).

In the vertebrate lungs, surface (free) macrophages protect the respiratory surface by phagocytosing pathogenic microorganisms (22, 131, 178) (Fig. 10*C*). The cells are so efficient that in disease-free lungs, the respiratory surface is practically sterile. Notwithstanding their protective role, macrophages can initiate and perpetuate a range of inflammatory diseases (22, 174). Surface macrophages occur in the amphibian lung (131, 244) but are reportedly lacking in the snake, *Boa constrictor*, lung (87). Interstitial and intravascular macrophages exist in the lungs of various species of birds and mammals (6, 21, 42, 146, 206). The interstitial space and the extracellular matrix of the blood-gas barrier, e.g., on the thicker side of the interalveolar septum of the mammalian lung, contain supportive and contractile elements such as collagen, elastic tissue, smooth muscle, and fibroblasts. Nerve axons occur in the interstitial space of the

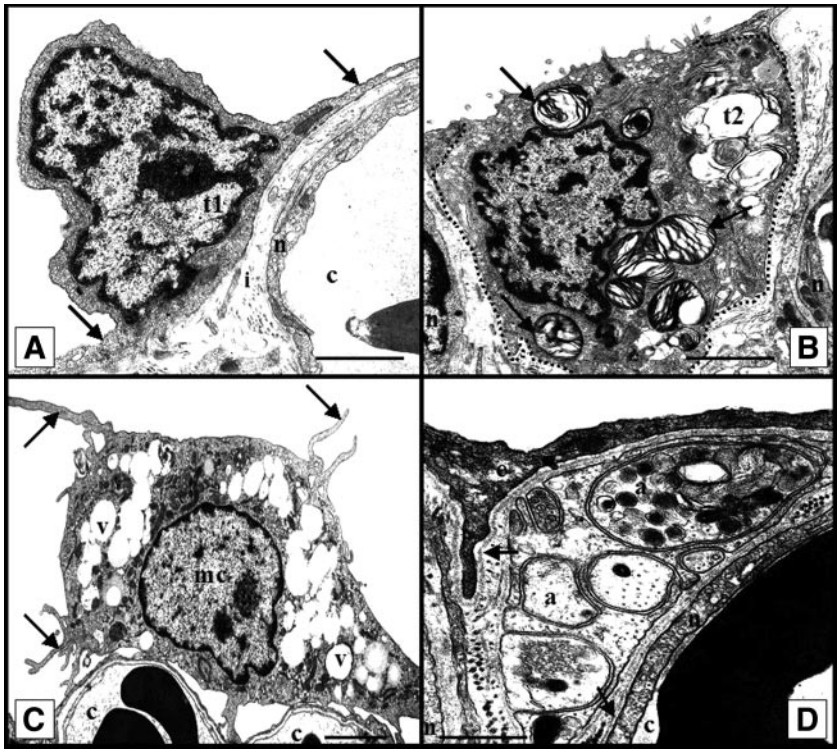

FIG. 10. *A*: type 1 epithelial cell (t1) of the lung of the tree frog, *Chiromantis petersi*, showing thin cytoplasmic extensions (arrows). i, Extracellular matrix; n, endothelial cell; c, blood vessel. Scale bar is 25 μm. [From Maina (142).] *B*: a type 2 epithelial cell (t2) of the lung of the tree frog, *Chiromantis petersi*, showing osmiophilic lamellated bodies (arrows). n, Endothelial cell. Scale bar is 1.5 μm. [From Maina (140).] *C*: alveolar macrophage (mc) of the lung of a bat, *Pipistrellus pipistrellus*. v, Vesicular bodies; arrows, filopodia; c, blood capillaries. Scale bar is 5 μm. *D*: surface of a faveolus of the lung of a snake, Black mamba, *Dendroaspis polylepis*, showing axonal profiles (a) in an interstitial space. e, Epithelial cell; n, endothelial cells; arrows, extracellular matrix; c, blood vessel. Scale bar is 5 μm. [From Maina (134).]

blood-gas barrier of the lungs of snakes (134) (Fig. 10*D*). With their long cytoplasmic extensions that contain numerous plasmalemmal or micropinocytotic vesicles, to an extent, endothelial cells resemble type 1 alveolar cells (Figs. 3, 4*A*, 5, 6, and 10, *A* and *D*). Epithelial cells are, however, less permeable to solutes and more selective to some ions (57). Endothelial cells constitute ~41% of the entire population of lung cells (40) and are significantly involved in the metabolic functions of the lung (7). The extracellular matrix (Figs. 3, 5, 6, and 10, *A*, *B*, and *D*) is deposited by the epithelial and endothelial cells. The matrix maintains the normal cytoarchitecture of the epithelial and endothelial cells, serves as a molecular barrier to negatively charged macromolecules, prevents passage of noninflammatory cells, and in certain cases influences cell differentiation, morphogenesis, and movement of molecular factors (41, 123, 204).

In the vertebrate lungs, notable differences occur in the extents of the differentiation and location of the pneumocytes. In the lungs of lungfishes (Dipnoi) and amphibians, the cells are incompletely differentiated; with microvilli on the apical surface, rather cuboidal in shape, and containing osmiophilic lamellated bodies, the pneumocytes have shared morphological features of fully differentiated type 1 and 2 pneumocytes (15, 175, 179). Pulmonary pneumocytes have completely differentiated into type 1 and type 2 cells in the avian (parabronchial) and mammalian (bronchioalveolar) lungs. The division of the cells may have greatly contributed to the thinning of the blood-gas barrier: the metabolically active type 2 cells adopted a cuboidal shape and hence came to line little of the blood-gas barrier, while the type 1 cells were rendered practically metabolically inert, became extremely attenuated, and covered most of the respiratory surface. Moreover, the process of fine-tuning the thickness of the blood-gas barrier entailed displacement of the epithelial cell bodies (perikarya) away from the blood-gas barrier to sites where the blood capillaries adjoined and the location of the connective tissue elements in nonrespiratory sites (Fig. 11). For example, in the avian lung, the cell bodies of the type 1 cells (Fig. 12*A*) infrequently occur on the respiratory surface and type 2 cells and surface macrophages are totally confined to the atria and infundibulae, "distant" nonrespiratory sites (116, 117, 146). The interalveolar septum of the mammalian lung has thick (supportive) and thin (respiratory) sides; connective tissue elements such as collagen and elastic tissue are found on the thicker side. The lungs of the ectothermic vertebrates have thicker barriers compared with those of the endothermic ones (75, 147, 168) (Table 1).

4. Sporadic attenuation in the design of the blood-gas barrier

In the mammalian lung, thin and thick sides occur at opposite sides of the interalveolar septum, while in the

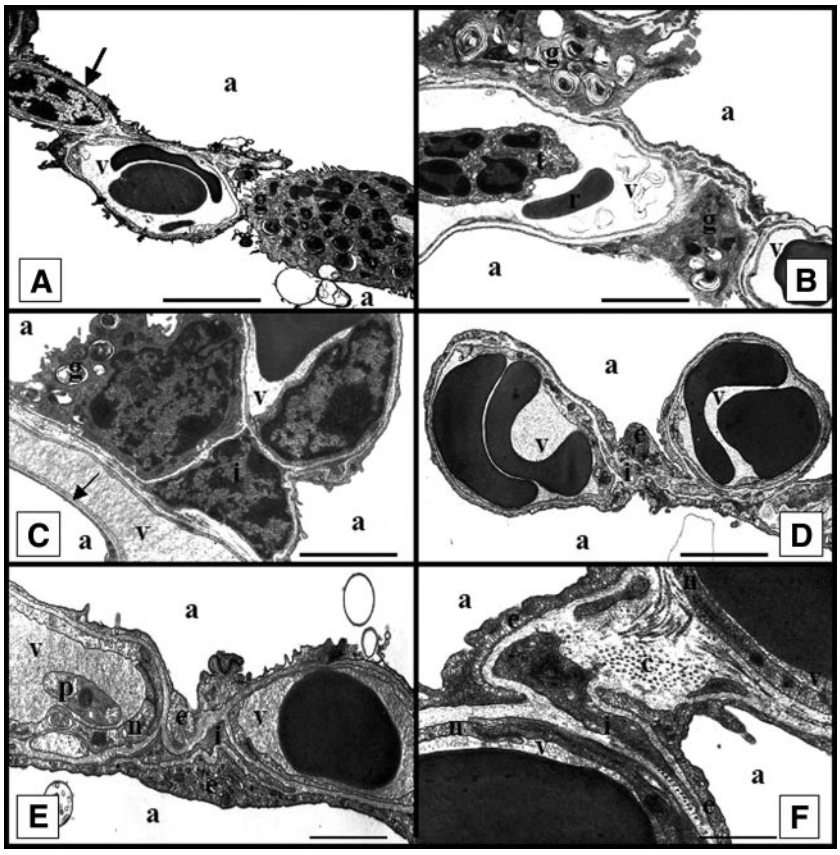

FIG. 11. *A*: an interstitial cell (arrow) and a granular pneumocyte (g) in a bat lung, *Epomophorus wahlbergi*. The cells are located away from a blood capillary (v). a, Alveoli. Scale bar is 10 μm. [From Maina et al. (152).] *B*: lung of a bushbaby, *Galago senegalensis*, showing type 2 (granular) pneumocytes (g) located at intercapillary junctions away from the blood-gas barrier. a, Alveoli; v, blood capillaries; t, a neutrophil. Scale bar is 5 μm. [From Maina (142).] *C*: lung of a bushbaby, *Galago senegalensis*, showing an interstitial cell (i) and a type 2 cell (g) located between blood capillaries (v). a, Alveoli. Scale bar is 8 μm. *D*: blood capillaries (v) in the lung of a bat, *Epomophorus wahlbergi*. i, Interstitial cell; e, epithelial cell. Scale bar is 15 μm. [From Maina et al. (152).] *E*: blood capillaries (v) in the lung of a bat, *Cynopterus brachyotis*. n, Endothelial cell; e, epithelial cell; i, interstitial cell; p, platelet; a, alveoli. Scale bar is 10 μm. *F*: junction between blood capillaries (v) in the lung of a vervet monkey, *Cercopithecus aethiopicus*, showing an interstitial cell (i) and collagen fibers (c). a, Alveoli; e, epithelial cell; n, endothelial cell. Scale bar is 3 μm.

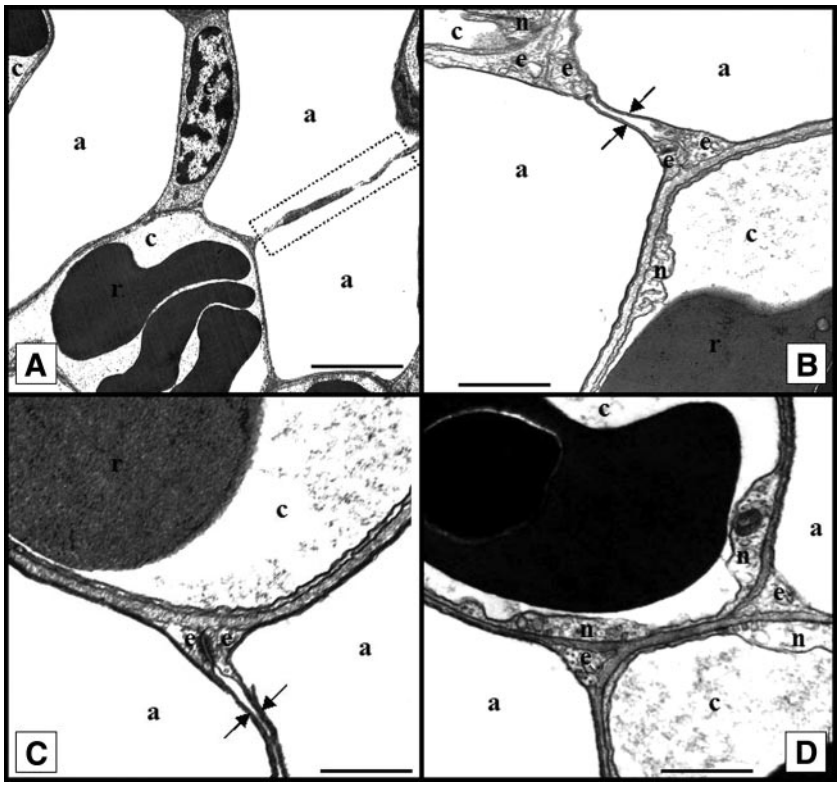

FIG. 12. *A*: lung of the graylag goose, *Anser anser*, showing a type 1 epithelial cell (e) and a necrotising one (boxed area). a, Air capillary; c, blood capillary. Scale bar is 10 μm. *B* and *C*: lung of a redwing, *Turdus olivaceus*, showing sites where air capillaries lie adjacent to each other and where epithelial cells (e and arrows) lie back to back: an extracellular matrix space is lacking in such sites. n, Endothelial cell; e, epithelial cell; c, blood capillary; r, red blood cell. Scale bars are 3 μm. *D*: lung of the blackheaded gull, *Larus ridibundus*, showing an area where blood capillaries (c) contact. Note the lack of cellular and connective tissue elements. n, Endothelial cell; e, epithelial cell; c, blood capillary. Scale bar is 2.5 μm. [From Maina and King (147).]

avian lung the blood-gas barrier (the tissue barrier between the air and the blood capillaries) is of even thickness, i.e., respiratory and supportive sides do not exist. In the parabronchial lung, however, while the extracellular matrix is of uniform thickness, the endothelial cell component of the blood-gas barrier presents conspicuous unevenness (Figs. 3 and 12, *B–D*). The irregularity produces extremely thin parts between relatively thicker ones. Weibel (237) envisaged that if the same quantity of structural material is utilized in the construction, periodic thinning of the blood-gas barrier allows the effective diffusion mean thickness of the barrier (the harmonic mean thickness, τ_{ht}) to be three times smaller than if it was of even thickness. Given that building a blood-gas barrier twice this increases the diffusing capacity by one-quarter of the original value (239), sporadic (irregular) design may be a compromise solution for enhancing respiratory efficiency while preserving structural integrity. The importance of uneven construction of the blood-gas barrier to respiratory function is reflected in the fact that the design occurs, though less conspicuously, in the water-blood barrier of the secondary lamellae of the fish gills (110) (Fig. 7, *B*, *D*, and *E*) and is particularly conspicuous in the lungs of the endothermic vertebrates, i.e., mammals and birds (147) (Figs. 5 and 6). In the mammalian lung, the degree of epithelial and endothelial cell attenuation is significantly greater on the thin side of the interalveolar septum, while epithelial cell attenuation is more marked than the endothelial one on the thick and thin sides (47). In the lungs of some vertebrate taxa, e.g., those of amphibians (168) and in the water-blood barrier of the secondary lamellae of the fish gills (110), an interstitial space is intercalated between the epithelial and endothelial cells; collagen and elastic tissue fibers, smooth muscle fibers, nerve fibers, lymphatic spaces, and fibroblasts occur (Figs. 5, *A* and *F*, 6*B*, 7, *D* and *E*, 10, *A* and *D*, and 11, *D–F*). In the thin respiratory parts of the interalveolar septum of the mammalian lung and in the blood-gas barrier of the avian lung, a thin extracellular matrix layer separates the epithelial and endothelial cells (Fig. 6). Interestingly, in the avian lung, in sites where air capillaries lie next to each other, epithelial cells lie back to back, with an extracellular matrix space lacking (Fig. 12, *B* and *C*). As demonstrated on the cells of the renal tubules by Welling and Grantham (243), on their own cells cannot tolerate significant tension. The lack of an extracellular matrix space between the epithelial and the endothelial cells in the sites where air capillaries lie adjacent to each other (areas that in the "fixed" lung should experience little tension) provides indirect evidence that at least in the avian lung, the stress-bearing component of the three-ply blood-gas barrier may be attributable to the extracellular matrix. This deduction is further supported by the fact that while the endothelial and epithelial cells manifest remarkable sporadic attenuation, the extracellular matrix maintains constant thickness (Fig. 6, *D–F*). The construction of the blood-gas barrier in the avian lung, where epithelial cells alone separate air capillaries, has been permitted by the rigidity

of the lung. Between the ventilatory cycles, the volume of the avian lung changes by a mere 1.4% (111). Suspended in a virtually inflexible construction, the areas where air capillaries lie adjacent to each other should expectedly be subjected to minimal tension.

C. Structural-Functional Correlations in the Design of the Blood-Gas Barrier

Before the 1940s when sound, reliable, and reproducible quantitative methods were formulated or modified from those used in disciplines like engineering and geology to analyze biological tissues (31, 34, 54, 55, 95, 230, 231), comparative pulmonary morphology was largely descriptive. Qualitative features like the degree of vascularity were used as relative indicators of respiratory efficiency. Plentiful comparative data now exist to allow far-reaching deductions to be made on the means and strategies that different animals utilize to procure molecular oxygen.

Pulmonary morphometric data show that the thickness of the water/blood-gas barrier correlates with properties such as body mass, phylogenetic stage of advancement , life-style pursued, and habitat occupied (51–53, 75, 105, 127, 132, 147, 148, 168, 191). Regarding the thickness of the blood-gas barrier, the most meaningful estimator of the diffusing capacity (or conductance) is the harmonic mean thickness (τ_{ht}). Determined from the reciprocal of the mean of the sum of the reciprocals of representative intercept length measurements that are taken orthogonally, i.e., perpendicular to the plane at which the blood-gas barrier has been sectioned (to offset the effect of obliqueness of tissue cutting) and ranked on a logarithmic scale to weight the smaller measurements (90, 232, 241), τ_{ht} is determined as

$$1/\tau_{ht} = 1/n \sum_{i=1}^{n} 1/1_i \quad (5)$$

where n is the total number of intercepts measured and $\sum_{i=1}^{n} 1/1_i$ is the sum of the reciprocals of the intercepts, i.e., the measurements of the thickness of the blood-gas barrier.

The emphasis of the thinner parts of the blood-gas barrier in the calculation of τ_{ht} makes practical sense in so far as much of the diffusion of oxygen across the blood-gas barrier occurs across such areas. It is vital to underscore that the τ_{ht} does not provide the absolute measure of the thinness of the blood-gas barrier and hence reflect its strength but rather defines the measure of the thickness that appropriately epitomizes the resistance (and hence the conductance) that the barrier presents to diffusing oxygen molecules. Estimation of the strength of the blood-gas barrier from the perspective of its thickness requires measurement of its thinnest parts and better still estimation of the surface area that such parts contribute to the entire measure (16). In accord to the well-known axiom (3), that "a chain is only as strong as its weakest link," it is a poor design for the blood-gas barrier to be too thin to tolerate tension under normal conditions of operation and to be too thick to meaningfully allow flux of oxygen by passive diffusion. Anticipated loading and necessary safety margin of operation should determine the overall design of the blood-gas barrier. An optimal design is one that confers adequate strength while allowing efficient diffusion.

The arithmetic mean thicknesses (τ_t) and the τ_{ht} in the amphibian, reptilian, and mammalian lungs differ substantially (75, 168, 188). Furthermore, except for the epithelial cell, the volume densities (proportions) of the components of the blood-gas barrier, i.e., the epithelium, interstitium/extracellular matrix, and the endothelium, vary. While in the three taxa the epithelium invariably forms 31% of the volume of the blood-gas barrier, in amphibians, reptiles, and mammals, respectively, the interstitium/extracellular matrix forms 43, 44, and 41% and the endothelium forms 26, 25, and 28% of it (168). In the avian lung, however, the endothelium constitutes much of the blood-gas barrier (67%), while the extracellular matrix and the epithelium comprise 21 and 12%, respectively (147). Although generally thicker than the blood-gas barrier of lungs, the water-blood barrier of the fish gills may be as thin as 0.2 μm in certain species (105, 122, 138). In the various vertebrate species examined by Meban (168), on average, the mean τ_t of the blood-gas barrier was 1.61 μm in the mammalian lung and, respectively, 2.17 and 2.04 μm in the amphibian and reptilian lungs. The minimum τ_{ht} of the blood-gas barrier in the avian lung is 0.068 μm (132, 147), that in mammalian lung is 0.20 μm (75), and the values in the reptilian and amphibian lungs are 0.22 and 0.21 μm, respectively (168).

The ratio of the τ_t to τ_{ht} defines the degree of attenuation and hence the unevenness of the thickness of the blood-gas barrier (241). In the vertebrate lung, the highest ratio (8:1) was reported in the avian lung by Maina and King (147). Corresponding values in the mammalian, reptilian, and amphibian lungs are, respectively, 3:1, 2:1, and 1.3:1 (169) (Table 1). Morphological observations show conspicuous corrugation of the blood-gas barrier of the avian lung (Figs. 5 and 6) compared with those of other vertebrates (Fig. 6, *D–F*); of the three structural components of the blood-gas barrier, the endothelial cell is markedly the most uneven.

The τ_{ht} in the lungs of various vertebrate taxa are given in Table 1. Among mammals, bats, the only volant taxon, generally have the thinnest barriers (149, 152, 159). The thinnest barrier (0.120 μm) has been reported in the lung of the flying fox, *Phyllostomus hastatus* (159).

Among the nonflying mammals, the remarkably small, metabolically highly active shrew, *Suncus etruscus* (65, 210), has the thinnest blood-gas barrier (0.23 μm) (76). In birds, the thinnest blood-gas barrier (0.099 μm) has been reported in the African rock martin, *Hirundo fuligula* (127), and the violet-eared hummingbird, *Colibri coruscans* (51), two small, highly energetic species. The generally small passerine birds, a highly successful group that comprises of ~5,739 species (>60% of the total number of extant avian species) (8, 207) and that operates at a relatively higher body temperature of 42°C compared with that of 40°C of other birds and the lower one of 38°C of mammals (5, 120), have relatively thinner blood-gas barriers (127). Exceptionally thick blood-gas barriers occur in the lungs of large, nonflying birds: τ_{ht} is 0.530 μm in the lung of the Humboldti penguin, *Spheniscus humboldti* (150); in the emu, *Dromaius novaehollandiae*, the value is 0.232 μm (151); in the domestic fowl, *Gallus gallus* variant *domesticus*, it is 0.318 μm (2); and in the ostrich, *Struthio camelus*, it measures 0.560 μm (158). The thick barrier in the penguin lung purportedly averts collapse of the air capillaries during dives (245). Among the air-breathing vertebrates on which data are available, the blood-gas barrier is thickest in the lungs of the low metabolism amphibians, the common newt, *Triturus vulgaris* (2.34 μm) and the Italian crested newt, *Triturus cristatus* (2.20 μm) (168); these animals utilize accessory respiratory structures like the skin and the buccal cavity to meet their overall oxygen needs.

1. *Optimization of the thickness of the blood-gas barrier*

In the vertebrate lungs, the thickness of the blood-gas barrier appears to have been allometrically optimized. This consideration is based on the fact that the parameter changes very little with increasing body mass (Fig. 13). Illustratively, although mammals span a colossal range of body mass from the minute 2.5 g Etruscan shrew, *S. etruscus*, to the ~150-ton bowhead whale, *Balaena mysticetus*, a factorial difference of $\sim 60 \times 10^6$, the thickness of the blood-gas barrier (τ_{ht}) of the lung of the shrew (0.230 μm) (76) differs from that of 0.350 μm (τ_t) of a whale (94) by a factor of only 1.3. In birds, the thickness of the blood-gas barrier in the 7.3 g violet-eared hummingbird, *Colibri coruscans* (the smallest bird on which data are available), is 0.099 μm (51), while that of an immature 40-kg ostrich, *Struthio camelus* (the heaviest bird on which τ_{ht} is available), is 0.56 μm (158); the body mass factorial difference is 5×10^3 while that of the thickness of the barrier is ~6. In bats where the heaviest species, the flying foxes, weigh ~1.5 kg, the thickness of the blood-gas barrier in the tiny 5 g pipistrelle, *Pipistrellus pipistrellus*, is 0.206 μm compared with that of 0.303 μm in *Pteropus poliocephalus* (149, 159); the body mass factorial difference is 185 while that of the thickness of the blood-gas barrier is only 1.5. The remarkable thinness of the blood-gas barrier in the avian lung together with paucity of surface (free) macrophages on the respiratory surface (116, 146, 178) are thought to predispose birds to pulmonary infections and pathological afflictions.

III. DESIGN OF THE BLOOD-GAS BARRIER FOR STRENGTH

A. Components of the Blood-Gas Barrier

Unless otherwise stated, this section will specifically address the blood-gas barrier of the mammalian lung. This

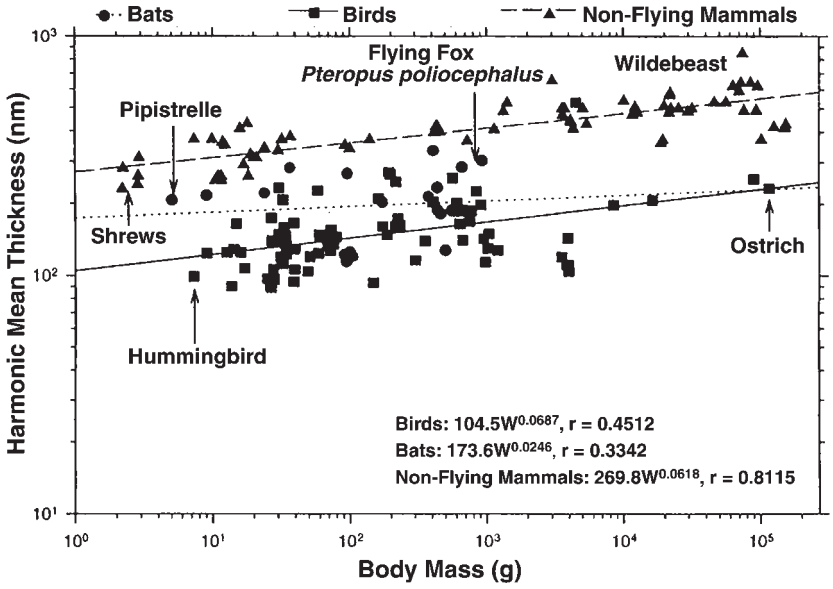

FIG. 13. Double logarithmic plot of the harmonic mean thickness of the blood-gas barrier (τ_{ht}) against body mass in birds, bats, and nonflying mammals. The very small slopes of the regression lines in the three vertebrate taxa indicate that τ_{ht} changes little with increasing body size. This suggests that the thickness of the tissue barrier may have been optimized for efficient gas exchange. [Bird data from Maina (132) and Maina et al. (153); bat data from Maina and King (149) and Maina et al. (159); nonflying mammal data from Gehr et al. (75).]

is unfortunately because hardly any data exist regarding the minimum thickness, strength, and failure of the blood-gas barrier in the lungs of the other vertebrate taxa. Indeed, even for the mammalian lung itself, details are only available for the dog, rabbit, rat, human, and horse (Thoroughbred) lungs.

In discussing the strength of the blood-gas barrier, we should first recognize the differences in the composition of the thin and thick sides of the interalveolar septum. In many lungs the blood-gas barrier is polarized in the sense that one side is extremely thin while the other side is substantially thicker. As pointed out in section II*B*, the thin side is made up of a fine protoplasmic extension of a type 1 alveolar cell, the thin cell body of a capillary endothelial cell, and an interstitium or extracellular matrix between these two cellular layers. Covering the alveolar epithelial layer is an aqueous surface lining layer containing pulmonary surfactant. This thin fluid layer with its very low surface tension makes only a small contribution to the strength of the barrier (176). The primary function of this thin side of the blood-gas barrier is to allow efficient gas exchange by passive diffusion, and this function requires its extreme thinness.

In contrast, the thick side of the blood-gas barrier apparently has other functions. Of course some gas exchange may occur across it, but because its thickness is several times that of the thin side, its diffusion resistance is high and its efficiency for gas exchange is low. One of its functions is to allow fluid exchange across the pulmonary capillary, and it is noteworthy that in early interstitial pulmonary edema, there is substantial thickening of this portion of the blood-gas barrier as a result of fluid accumulation, while there are no morphological changes on the thin side (63, 217). Here it should be emphasized that fluid apparently moves out of the pulmonary capillary into the interstitium whenever the capillary pressure rises. For example, Staub (211) showed in awake sheep that very soon after an intravenous infusion of saline or dextran there is a measurable rise in lymph flow from the lung as would be expected from the disturbance of the Starling equilibrium. Indeed, it is likely that on exercise, the inevitable rise in pulmonary capillary pressure will result in fluid movement out of the capillary into the interstitium of the lung, and at the end of the exercise when the capillary pressure falls, the fluid will reenter the capillary from the interstitium.

The thick side of the blood-gas barrier has an additional function as emphasized by Weibel (234). It accommodates the type I collagen fibers that make a major contribution to the structural scaffolding of the lung in the alveolar region and elsewhere. These fibers thread their way along the alveolar wall, crossing from one side to the other, and as they pass adjacent to a capillary lumen they are accommodated in the thick side of the blood-gas barrier. This anatomical arrangement is responsible for the polarization of the blood-gas barrier because the region containing the type I collagen fibers needs to be relatively wide to accommodate them, while on the other side of the capillary lumen in the absence of these fibers, the barrier can afford to be extremely thin. The extracellular matrix on the thin side presumably plays little role in maintaining the shape of the alveolar region of the lung, but it is crucial in maintaining the integrity of the blood-gas barrier itself so that it can withstand the stresses resulting from increases in capillary transmural pressure or the longitudinal tension in the alveolar wall.

The structural scaffold resulting from the type I collagen fibers is anchored at the hilum and forms a support for both the airways and blood vessels as it penetrates deeper into the lung. One of its functions is to divide the lung into a series of lobes and bronchopulmonary segments. At the alveolar level, this fibrous network is responsible for maintaining the geometry of the alveolar ducts and the alveoli themselves. For example, the intraacinar airways including the respiratory bronchioles and alveolar ducts contain abundant fibers that make a mesh encircling the mouths of the alveoli. The concentration of the type I collagen of the connective tissue is particularly strong in the rings that demarcate the alveolar ducts.

It is generally assumed that the most vulnerable region of the blood-gas barrier from the point of view of mechanical integrity is the thin side because, other things being equal, the stresses will be highest there. However, it should be emphasized that the distribution of stresses on the thick side is unknown. In fact, ultrastructural studies of stress failure of pulmonary capillaries sometimes show disruptions on the thick side of the blood-gas barrier (for example, see Fig. 19*B*), emphasizing that our knowledge of the distribution of stresses is incomplete.

Many morphometric studies have been carried out on the thickness of the blood-gas barrier (74, 75, 234) (see Table 1), but unfortunately few of these give direct information about the distribution of thickness of the thin side of the barrier where we can expect the stresses to be highest. The reason for this odd state of affairs is that most morphometrists have concentrated on the performance of the lung for gas exchange, and in particular the structural factors determining the pulmonary diffusing capacity. As a consequence, they have rightly argued that some diffusion will occur across the thick side of the blood-gas barrier, and they have calculated the harmonic mean thickness inclusively (e.g., Ref. 74) (see sect. II*C*) (Table 1). This is indeed the appropriate measurement, since the diffusing capacity is inversely proportional to the thickness of the barrier, other things being equal. However, as pointed out in section II*C*, it is important to reemphasize that the harmonic mean thickness of the blood-gas barrier does not give direct information about the thickness of the thin side of the barrier, and in particular the distribution of the thicknesses of that side.

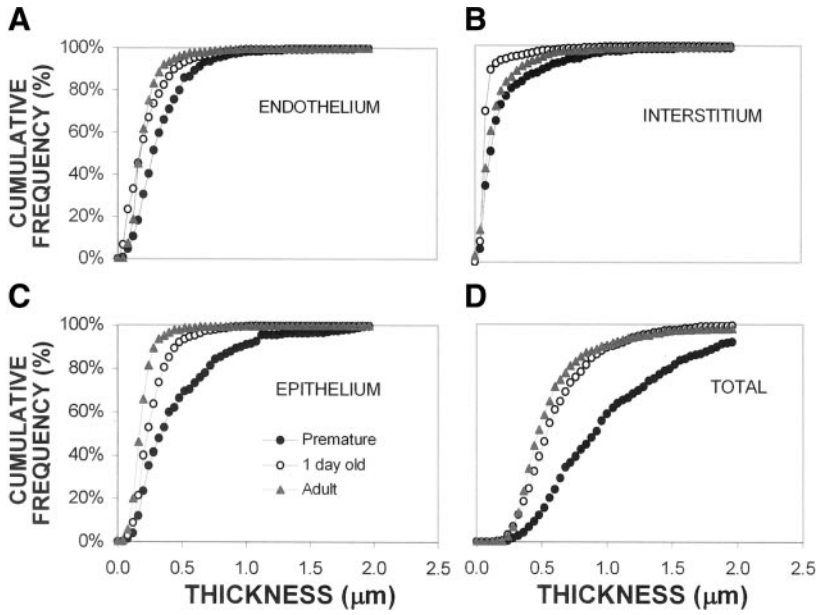

FIG. 14. Cumulative relative frequencies of the thickness of the endothelial (*A*), interstitial (*B*), and epithelial (*C*) layers and the total blood-gas barrier (*D*) of premature, 1-day-old, and adult rabbit lungs. These data show that the percentage of occurrence of very thin interstitium (0–0.1 μm) was much higher in 1-day-old rabbits (71.7 $\pm$ 5.2) than premature animals (35.3 $\pm$ 9.4) or adult animals (43.0 $\pm$ 2.6). This type of plot clarifies how much of the blood-gas barrier is extremely thin. [From Fu et al. (70).]

Essentially, the only studies that have addressed this problem are those by Birks et al. (16, 17) and Fu et al. (70) where random orthogonal measurements of the thin side of the blood-gas barrier were collated to give a distribution of thicknesses. The data were analyzed to show both the distribution of the number of measurements having particular thicknesses, and also a plot of cumulative thicknesses. These studies allow statements about the percentage of the portions of the thin side of the blood-gas barrier that have a thickness less than a given value.

As an example of this type of measurement, Fu et al. (70) showed that in newborn rabbits, 71.7% of the measurements of the interstitium of the thin side of the blood-gas barrier had a thickness of <0.1 μm, indicating a likely vulnerability to stress failure (Fig. 14). This result occurred in spite of the fact that the mean thicknesses of the blood-gas barrier between 1-day-old and adult rabbits showed no significant differences. This prediction of increased vulnerability in 1-day-old animals was confirmed when measurements were made of the number of disruptions of the blood-gas barrier as the capillary pressure was increased compared with adult rabbits (69). For comprehensive understanding of stress tolerance, it would be very valuable to have more data on the frequency distribution of thicknesses of the thin side of the blood-gas barrier and the proportion of the total respiratory surface area that the regions of extreme thinness constitute in other species of animals.

B. Molecular Composition of the Extracellular Matrix

The term *extracellular matrix* here refers to all the tissue, collagenous and noncollagenous, between the bilipid cell membranes of the alveolar epithelial cell and the capillary endothelial cell on the thin side of the blood-gas barrier. The reason for discussing the extracellular matrix is that, as described later, there is evidence that the strength of the thin side of the blood-gas barrier comes primarily from the basement membranes of the extracellular matrix.

The principal components of the extracellular matrix include the following: *1*) type IV collagen, *2*) laminin, *3*) entactin/nidogen, *4*) heparan sulfate proteoglycans, *5*) tenascin, and *6*) integrins and other anchoring fibers. Type IV collagen appears to be the most important molecule for the strength of the blood-gas barrier.

The type IV collagen in alveolar wall basement membranes has three polypeptide chains, two α1(IV) with one α2(IV), and is a threadlike structure made up of a triple helix. Each molecule is ~400 nm long and has a large COOH-terminal noncollagenous globular domain (NC1) at one end and a distinctive collagenous NH_2 terminal at the other end (7 S) that promotes cross-linking (Fig. 15). Two

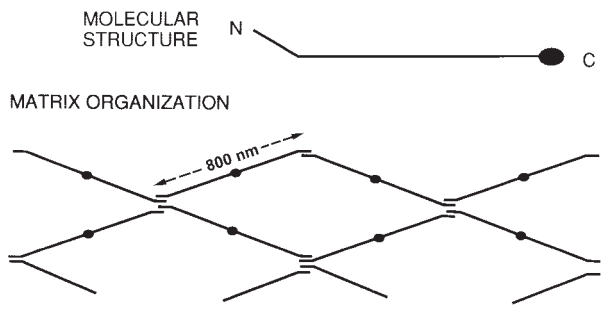

FIG. 15. Some features of type IV collagen. Each molecule is ~400 nm long. Two molecules join at the COOH terminal and four at the NH_2 terminal to give a matrix structure. [Modified from Timpl et al. (221).]

of the molecules link at the COOH terminus to give a doublet 800 nm long. Four molecules link at the NH_2 terminus to give a characteristic matrix or chicken wire structure (Fig. 15). This arrangement apparently combines great strength with porosity.

An interesting feature of human type IV collagen is that there are biochemical regions that may allow bending of the molecule. Takami et al. (218) described 25 irregularly spaced sites that may impart flexibility to the structure. In addition, a 90-nm-long segment of high flexibility near the 7S domain, which is rich in nontriple helical regions, has also been reported (96). Schwarz et al. (205) found frequent interruptions of the central domain by nontriple helical regions characterized by an imperfect GLY-XAA-YAA sequence repeat. These features are of particular interest in the context of basement membrane because of indirect evidence discussed below that the matrix configuration may distort when exposed to high stresses. The fact that the same locations for flexibility are seen in different species (18) is evidence for their functional importance.

Type IV collagen is believed to be synthesized by a variety of cells including endothelial cells, epithelial cells, and, in smaller amounts, by a number of mesenchymal cells. Procollagen synthesis is primarily determined by the steady-state level of procollagen mRNA which reflects a dynamic equilibrium between the rate of procollagen gene transcription, mRNA processing, and mRNA degradation. A number of factors regulate procollagen metabolism in cell culture, one of the most important being transforming growth factor (TGF)-β_1. This upregulates collagen deposition via a series of interlinked actions and is produced by a number of different cells including mesenchymal, epithelial, and chemopoietic cells. Type IV collagen along with other collagens presumably undergoes degradation and synthesis so that there is a tight balance between these processes. Many other types of collagen are known to be present in lung tissue, the total number of varieties being at least 11.

An important function of type IV collagen is that it serves as an anchoring structure for overlying cells. For example, studies have shown that a fragment of the collagen IV molecule located ~100 nm from the NH_2 terminus contains the binding sites for the integrins $\alpha1\beta1$ and $\alpha2\beta1$ (114).

Laminins constitute one of the most abundant groups of glycoproteins in basement membranes. They have a cross shape with three short arms ~37 nm long and one long arm of ~77 nm (60). The three short arms of laminin 1 are composed of a α_1-chain, β_3-chain, and γ_2-chain, respectively, although there are differences in terminology, and these then extend down the long arm as a triple helical coiled coil structure. Several different laminins are known and are assembled from genetically distinct α-, β-, and γ-chains. Laminins interact with a variety of cells and promote attachment, differentiation, and motility (115). For example, they are involved in stimulating neurons to form axonlike processes, they help endothelial cells to align and form capillary-like structures, and they interact with malignant tumor cells affecting tissue invasion and metastases.

Entactin/nidogen is a macromolecule that goes by both names because of its discovery in two different laboratories. It is shaped like a dumbbell with two globular domains at each end connected by a short (~17 nm) rod. The functions of entactin/nidogen are still unclear, but the molecule appears to have a tight association with laminin, occurring in equimolar concentrations with this molecule. Abnormalities of entactin/nidogen are associated with disturbances of the development of kidney and lung in vitro, suggesting that the molecule has a role in organ morphogenesis. The molecule may also bind to both type IV collagen and heparan sulfate proteoglycans.

Perlecan is the name given to a molecule consisting of a large proteoglycan core with long heparan sulfate chains attached to one end. Studies of heparan sulfate proteoglycans indicate that they have a major role in glomerular basement membranes where they form a negatively charged shield that prevents the loss of negatively charged serum proteins. These molecules have also been identified in alveolar basement membranes, but their function is unclear. It has been suggested that interactions of perlecan with type IV collagen, laminin, and entactin/nidogen are important in stabilizing basement membranes.

Tenascin, also known as tenascin-cytotactin (TN-C), is a family of extracellular matrix proteins that is unique in that the molecules form hexamers with a 6-arm structure as a result of assembly at the NH_2 terminus of the molecule. This structure allows them to interact with a variety of other extracellular matrix proteins including integrins and other adhesion molecules, fibronectin, and sulfate proteoglycans. The molecule is expressed strongly during embryogenesis and presumably has important functions in morphogenesis. Tenascins are active in wound healing but are apparently minimally expressed in normal adult tissues.

Integrins are adhesion molecules both in the extracellular matrix and also between adjacent cells. They link with the actin microfilament system of the cell cytoskeleton through a variety of proteins including vinculin, talin, α-actinin, and paxillin. Other anchoring fibers exist in extracellular matrix and sometimes form a characteristic banding pattern in electron micrographs with arrays that are perpendicular to the basement membrane (see Fig. 16*A*). Type VII collagen is a component of some of the anchoring fibers.

A feature of the extracellular matrix is that it undergoes constant remodeling, which involves breakdown of existing molecules and synthesis and deposition of new

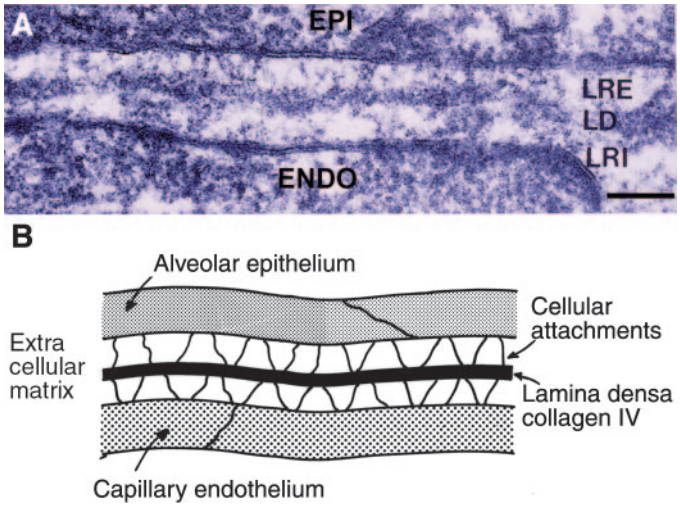

FIG. 16. *A*: high-power electron micrograph showing an electron-dense band called the lamina densa in the center of the extracellular matrix of the thin part of the blood-gas barrier. Most of the type IV collagen is believed to be located in the lamina densa (LD). EPI, epithelial cell; ENDO, endothelial cell; LRE, lamina rara externa; LRI, lamina rara interna. Bar is 0.1 μm. [Modified from Vaccaro and Brody (225).] *B*: diagram of the thin side of the blood-gas barrier. [Modified from West and Mathieu-Costello (250).]

proteins. Matrix metalloproteinases (MMPs) play a dominant role in the degradation of extracellular matrix. They are essential in development, tissue remodeling, and tissue repair. MMPs can be produced by a large range of cells including normal epithelial cells, fibroblasts, myofibroblasts, endothelial cells, and leukocytes.

C. What Component of the Blood-Gas Barrier Is Responsible for Its Strength?

As stated earlier, there is good though indirect evidence that the strength of the blood-gas barrier comes not from the alveolar epithelial or capillary endothelial layers themselves, but from the extracellular matrix between them and in particular their basement membranes. The evidence for this is discussed below.

The most extensive study to date giving information about the mechanical properties of basement membrane is that by Fisher and Wakely (62), who measured several variables including the ultimate tensile strength and Young's modulus of basement membrane from the lens capsule of the cat. It should be pointed out that this particular basement membrane is ~15 μm thick, which is some 150 times thicker than the basement membranes in the blood-gas barrier, so there may be differences in molecular structure. The value for ultimate tensile strength was $1.74 \pm 0.16 \times 10^6$ N/m^2. It is interesting that this high figure is comparable with that reported for cow ligamentum nuchae which is composed principally of type I collagen where the value was 2×10^6 N/m^2 (208). Another study of the ultimate tensile strength of mouse type I collagen gave a value of $6–7 \times 10^6$ N/m^2 (214). There are marked differences between the fibrillary structure of collagen I and the matrix organization of collagen IV (Fig. 15), so it is perhaps remarkable that their mechanical strength is so similar.

Additional information on the ultimate tensile strength of basement membrane comes from measurements of Welling and Grantham (243) who attached isolated rabbit renal tubules to micropipettes and increased the pressure within them while measuring their change in diameter. These investigators were not able to obtain a direct measurement of ultimate tensile strength because the tubules separated from the micropipettes before they failed, but as seen in their Table 1, experiment 39, they showed that a tubule with a diameter of 57 μm and wall thickness of 0.26 μm could withstand a transmural pressure of 42 cmH_2O (31 mmHg = 4.1 kPa). With the use of the Laplace relationship, this means that the ultimate tensile strength exceeded 5×10^5 N/m^2. This result is generally consistent with the results of Fisher and Wakely (62) discussed above.

The isolated rabbit renal tubules studied by Welling and Grantham (243) were composed of only a single epithelial layer and its basement membrane. The authors made an additional important observation when they showed that the relationship between the transmural pressure and the diameter of the renal tubule was the same whether or not the epithelial layer was removed with detergent. This is strong evidence that the single layer of epithelial cells did not contribute to the mechanical properties in extension. The experiment also provides good evidence that the considerable strength of the renal tubule comes from the basement membrane.

Additional studies supporting the role of basement membrane in determining mechanical properties of capillaries come from the work of Swayne et al. (216), who showed that the distension of capillaries in frog mesentery was consistent with the elastic properties of basement membrane. However, these results should be interpreted with caution because Fung (71) has pointed out that mesenteric capillaries can receive considerable support from the soft tissue surrounding them, and this may be more important in their mechanical behavior than the structure of the capillary wall itself.

There is other indirect evidence that basement membrane is an important structure in the mechanical behavior of capillaries. For example, it has been shown that the thickness of basement membrane in systemic capillaries is related to the hydrostatic pressure within them. Williamson et al. (257) reported that the thickness of the basement membrane increased from the abdomen to the thigh to the calf in humans, and they also showed a progression from shoulder to leg in the giraffe! It is known that glomerular capillaries normally withstand a high

transmural pressure of the order of 35–40 mmHg (4.7–5.3 kPa) (26) and that they have very thick basement membranes, for example, 350–400 nm in human kidney, that is 3–4 times greater than in pulmonary capillaries. In Goodpasture's syndrome where antibodies attack the NC1 globular domain of type IV collagen (256), bleeding occurs into both the glomerular and alveolar spaces, again suggesting that basement membrane plays a critical role in the mechanical integrity of the capillary. In the pathological condition known as "thin basement membrane nephropathy," there is persistent glomerular bleeding in both children and adults (201). Additional evidence is that when the blood-gas barrier fails, a common pattern is disruption of either the alveolar epithelial or capillary endothelial layers with preservation of basement membrane (see Fig. 19, *A* and *B*). As mentioned in section II*B4*, in the avian lung, while conspicuous sporadic attenuation occurs in the endothelial cell of the blood-gas barrier, the extracellular matrix is constant in thickness (Fig. 6, *D–F*). Moreover, in areas where air capillaries lie next to each other, sites that in the fixed avian lung should not be subjected to stress, an extracellular matrix and therefore a basement membrane is lacking (Fig. 12, *C* and *D*).

The evidence that basement membrane plays a dominant role in the strength of capillary walls generally, and the blood-gas barrier in particular, seems strong. However, it must be conceded that we only have indirect evidence that it is the type IV collagen in the basement membrane that is responsible for the mechanical strength. It has not been feasible to make measurements on pure type IV collagen. Studies on tendons including human calcaneal tendon which is primarily composed of type I collagen (259), and mouse collagen (208, 214), have given very high values of ultimate tensile strength, but of course while type IV and type I collagens have some molecular similarities, they are certainly not identical. It could be argued that the role of type IV collagen in determining the strength of basement membrane is by default in that it seems unlikely that the other components listed earlier including laminin, entactin/nidogen, heparan proteoglycans, and tenascin do not have structures suggesting great mechanical strength.

The morphology of the basement membranes in the thin side of the blood-gas barrier is remarkable (Fig. 16). High-power electron micrographs show that whereas the individual basement membranes of the alveolar epithelial cell and capillary endothelial cell lie close to their respective cell surfaces in the thick part of the blood-gas barrier, and therefore are separated by most of the rest of the extracellular matrix, a different appearance is seen on the thin side of the blood-gas barrier. Here the two basement membranes fuse in the center of the extracellular matrix forming an electron-dense layer presumably because of the high electron density of type IV collagen (Figs. 5 and 6). Figure 16 particularly shows the lamina densa (LD) in the center of the extracellular matrix with the lamina rara externa (LRE) on the epithelial side and the lamina rara interna (LRI) on the endothelial side. Cellular attachments made up of anchoring fibers can be seen running across both the LRE and LRI, often perpendicular to the basement membrane. Other evidence for the central location of type IV collagen in the middle of the extracellular matrix has been provided by Crouch et al. (41) who used anti-human type IV collagen antibody and showed that the distribution of this was closely associated with the LD seen by electron microscopy (Fig. 17).

A striking feature of the LD is its extreme thinness, certainly <50 nm in many parts of Figure 16*A*. Note that the bar is 0.1 μm or 100 nm. It is very remarkable that this extremely thin layer of strong type IV collagen acts as our lifeline protecting the integrity of the blood-gas barrier, and thus preventing the leakage of blood components into the alveolar space under all but the most extreme physiological conditions discussed below.

An interesting implication of the appearances shown in Figure 16 is that the type IV collagen matrix shown in Figure 15 must be oriented parallel to the epithelial and endothelial cell surfaces. This is because each single molecule of type IV collagen is 400 nm long, and the doublet is twice this. Clearly, there is not enough space to accommodate these large molecules in the lamina densa only 50 nm thick unless the matrix was in the same plane as the surfaces of the endothelial and epithelial cells. An analogy is the appearance obtained if sheets of chicken wire are placed on top of each other on a flat floor. The thickness of the wire sheets would be very small, but their strength in extension along the floor surface would be great.

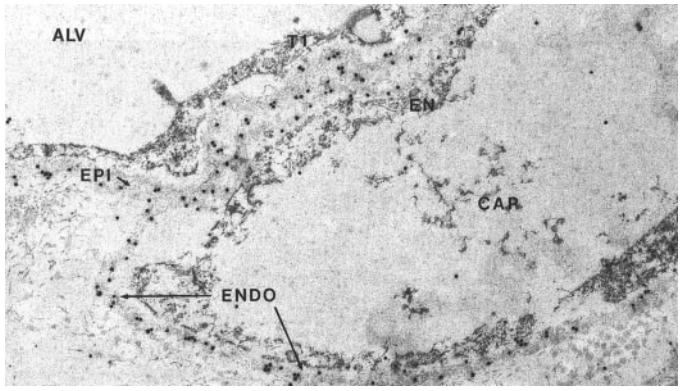

FIG. 17. Distribution of type IV collagen in epithelial basement membrane (EPI) and endothelial basement membrane (ENDO) of human lung using anti-human type IV collagen antibody. ALV, alveolus; CAP, capillary. Note that the type IV collagen indicated by immunocytochemistry tracks the electron-dense layers and is predominantly located in the center of the extracellular matrix (compare with Fig. 16). [From Crouch et al. (41).]

D. Stresses in the Blood-Gas Barrier

Two mechanisms by which stresses are developed in the blood-gas barrier are shown in Figure 18. The first is the hoop or circumferential stress that develops as a result of the transmural pressure difference acting across the curved capillary wall according to the Laplace relationship. We can regard the capillary as part of the thin-walled cylindrical tube in which case the hoop stress S is given by

$$\frac{Pr}{t}$$

where P is the transmural pressure, r is the radius of the capillary, and t is the thickness of the load-bearing structure.

The second mechanism for raising the stress in the blood-gas barrier is increased tension in the alveolar wall when the lung is inflated. In this context we can think of the alveolar wall as a string of capillaries with part of the longitudinal tension of the wall being transmitted to the capillary wall. It is true that the type I collagen fiber scaffolding that runs through the thick portion of the blood-gas barrier almost certainly bears some of these loads. Nevertheless, we know that when the lung is inflated to high volumes the diameter of the capillaries orthogonal to the alveolar wall is markedly reduced if the transmural pressure of the capillaries remains constant (77). Further evidence of an increase in capillary wall stress at high lung volumes is that the frequency of stress failure of the blood-gas barrier is greatly increased, again for the same capillary transmural pressure (68).

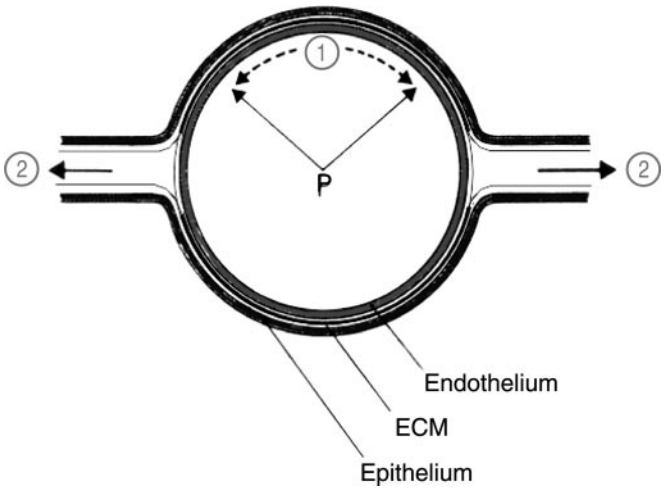

FIG. 18. Diagram showing two mechanisms that can cause an increased stress in the blood-gas barrier. *1*, Hoop or circumferential stress caused by the capillary transmural pressure; *2*, results from linear tension in the alveolar wall which increases as the lung is inflated. P, capillary hydrostatic pressure. [Modified from West et al. (253).]

A third though minor factor that apparently influences hoop stress is the surface tension of the alveolar lining layer. When the capillaries protrude into the alveolar space as a result of a high capillary transmural pressure, there is evidence that the surface tension protects them from stress failure to some extent (176). This factor will not be present unless the capillaries bulge outward as shown histologically in Figure 1*D* of Glazier et al. (77) and diagrammatically in Figure 18 of this review. To quantify the supportive role of surface tension, ultrastructural studies were carried out on both air-filled and saline-filled lungs at the same capillary transmural pressures and lung volumes (176). Saline filling was used to abolish the normal air-liquid surface tension. The results showed that the frequency of breaks in the endothelium was not significantly different between air and saline filling and that there were actually fewer breaks in the outer boundary of the epithelial cells with saline filling. In contrast, a larger number of breaks were seen in the inner boundary of the epithelium in the saline-filled lungs. These results are difficult to interpret but suggest that the role of surface tension is generally small but that not all portions of the blood-gas barrier are subjected to the same tensile forces. In interpreting these data it should be pointed out that the measurements were made in air-filled lung at a normal transpulmonary pressure of 5 cmH_2O, and the same lung volume was used for saline filling. However, the surface tension of the alveolar lining layer varies considerably with lung volume being as high as 30 mN/m (dyn/cm) at total lung capacity but only about 1–2 mN/m at functional residual capacity (6a).

It is instructive to calculate the approximate hoop stress in the blood-gas barrier of the human lung during severe exercise. Although capillary pressures have not been measured directly, mean pulmonary artery pressure has been shown to increase from ~13 mmHg (1.7 kPa) at rest to as much as 37 mmHg (4.9 kPa) during severe exercise (58, 89, 229). Pulmonary arterial wedge pressures as a measure of venous pressure have been measured as high as 21–30 mmHg (2.8–4.0 kPa) (199, 229). Although the exact relationship between pulmonary capillary, arterial, and venous pressures is not known, micropuncture studies of pressures in small pulmonary blood vessels in anesthetized cats have shown that the capillary pressure is about halfway between arterial and venous pressure, and more importantly, much of the pressure drop occurs in the capillary bed (14). The implication is that at midlung during heavy exercise, the mean capillary pressure is at least 30 mmHg (4.0 kPa), although some capillaries at the upstream end of the bed will be exposed to a higher pressure. If we now add the hydrostatic gradient to capillaries at the bottom of the upright lung, we end up with a capillary pressure of ~36 mmHg (4.8 kPa) (253). Alveolar pressure on the other side of the

capillary will fluctuate a little with inspiration and expiration, but the mean is close to atmospheric pressure.

There are no data on the radius of human pulmonary capillaries at high capillary pressures, but using average measurements from rabbits and dogs gives a value of 3.5 μm (16). The most elusive number is the thickness of the load-bearing structure. However, with the assumption that the type IV collagen is mainly limited to the electron-dense layer in the middle of the extracellular matrix (Fig. 15*A*), the thickness is ~50 nm and even less in some places. Inserting these numbers into the Laplace relationship given above gives a tensile stress in the layer of type IV collagen of $\sim 3 \times 10^5$ N/m^2, which is of the same order of magnitude as the ultimate tensile strength of the collagen as discussed earlier. The implication is that the normal lung does not have a great deal of reserve in terms of the strength of the blood-gas barrier, and this is consistent with evidence for changes in the integrity of the capillary wall that occurs in elite human athletes at high levels of exercise as discussed below. It is not possible to make a similar calculation for the longitudinal stress shown in Figure 3 because the relationship between lung inflation and the increased tension exerted on the capillary wall is unknown.

E. Patterns of Stress Failure

When the blood-gas barrier is subjected to unphysiologically high stresses it fails, that is, ultrastructural damage can be identified using electron microscopy. The term *failure* comes from engineering where a structure may fail if it is exposed to an unduly high load. The failure can take many forms, an example being the roof of a house if large amounts of heavy snow accumulate on it. The roof may sag, crack, buckle, or even collapse completely. Failure is a useful umbrella term because it includes all types of damage caused by abnormally high stresses.

The first studies on stress failure of pulmonary capillaries in our laboratory were carried out because of the puzzle posed by the mechanism of high-altitude pulmonary edema. It was known that the alveolar edema fluid in this condition had a very high protein concentration and that it contained many cells, indicating that there was damage to the walls of the pulmonary capillaries (203). It was also known that high-altitude pulmonary edema tended to be associated with unusually high pulmonary artery pressures, and we postulated that some of this pressure might be transmitted to the capillaries. To investigate the possible consequences of this, experiments were carried out on anesthetized open-chested rabbits where the pulmonary artery and left atrium were cannulated, and the lung was perfused with blood at an accurately known capillary transmural pressure. The lung was then perfusion-fixed using buffered glutaraldehyde and examined by electron microscopy (223, 253).

Figure 19 shows examples of the appearances. In Figure 19*A* disruption of the capillary endothelial cell can be seen, although the alveolar epithelial cell is normal and the basement membranes of the two cells are intact. Close scrutiny of the free ends of the disrupted endothelial cell shows that these are well-formed, suggesting that the bilipid cell membrane has been reconstituted. Figure 19*B* shows disruption of an alveolar epithelial cell near the top of the micrograph, although the basement membrane remains intact. Note the large degree of separation of the two ends of the cell. Near the bottom of the micrograph there is a smaller disruption of the capillary endothelial cell with the two ends marked by arrows. A blood platelet is in close proximity to the exposed basement membrane, and this is not surprising because the membrane is electrically charged, highly reactive, and attractive to cells.

Figure 19*C* shows complete disruption of the capillary wall with the two broken ends clearly visible and a red blood cell apparently moving out of the capillary into the alveolar space where two other red blood cells can already be seen. Figure 19*D* is a scanning electron micrograph of the surface of the alveolar wall showing breaks in the epithelial cells.

The characteristics of the cellular disruptions have been studied in detail (223). In these experiments a few breaks were seen at a capillary transmural pressure of 32.5 cmH_2O (24 mmHg = 3.2 kPa), but the number of breaks was much increased at a transmural pressure of 52.5 cmH_2O (39 mmHg = 5.2 kPa), and further breaks were seen at higher pressures. The length of the endothelial breaks on the transmission electron micrographs was between 1 and 2 μm, while the epithelial breaks were up to 3 μm long.

An important question is whether the breaks occur at the junctions between cells or within the cells themselves. For the epithelial cells, the scanning electron micrographs (for example, Fig. 19*D*) clearly show that the breaks are not at the intercellular junctions but within the cells themselves (37). This is perhaps consistent with the known highly organized tight junctions between adjacent epithelial cells (202). It was interesting that many of the breaks occurred very near the junctions, and we postulated that this might indicate a concentration of stresses in that area. The scanning electron micrographs also allowed the shapes and sizes of the breaks on the surface of the endothelial cells to be determined. Some 90% of the breaks were elongated with the remainder being roughly circular. The dimensions of the elongated breaks of the epithelium were ~4 μm in length and 1 μm in width, and the dimensions varied little with pressure.

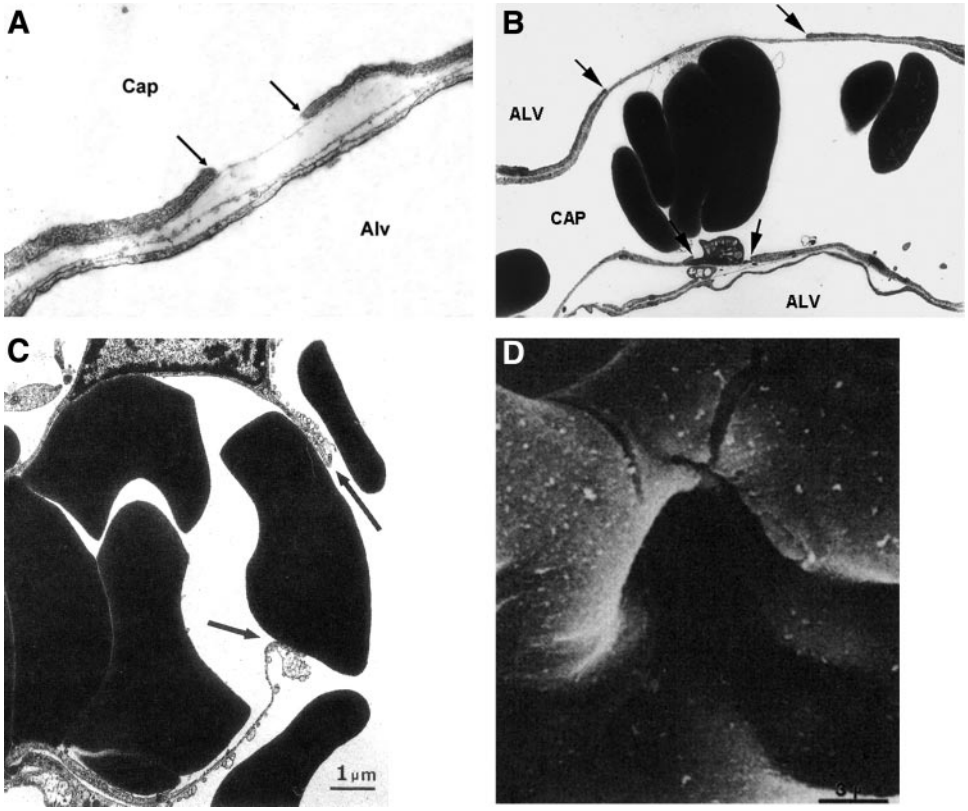

FIG. 19. Examples of stress failure in pulmonary capillaries. *A*: disruption of the capillary endothelial cell (arrows) but the alveolar epithelium and two basement membranes are intact. *B*: disruption of an alveolar epithelial cell at the top (arrows), and disruption of a capillary endothelial cell near the bottom (arrows). A blood platelet is adhering to the exposed basement membrane below. *C*: disruption of all layers of the capillary wall with a red blood cell apparently passing through the opening. *D*: scanning electron micrograph showing breaks in the alveolar epithelium. [*A* and *B* modified from West et al. (253); *C* from Tsukimoto et al. (223); *D* from West and Mathieu-Costello (251).]

Whether the disruptions of the endothelium occur at intercellular junctions or within cells is not possible to determine from these studies. However, other investigators have clearly shown that intracellular disruptions in endothelial cells can occur. Neal and Michel (177) increased the pressure in the capillaries of frog mesentery and used electron micrographs to make three-dimensional reconstructions. They found breaks in the endothelium that were transcellular and in fact reported that >80% of the breaks were transcellular rather than intercellular. It is interesting that these investigators also reported that the mesenteric capillaries began to fail at a transmural pressure of ~30 cmH_2O (22 mmHg = 3 kPa), which is similar to that required to cause breaks in the rabbit pulmonary capillaries.

A striking feature of the disruptions of the pulmonary capillaries is that many are rapidly reversible when the capillary transmural pressure is reduced. For example, Elliott et al. (59) raised the pressure to 52.5 cmH_2O (39 mmHg = 5.2 kPa) for 1 min of blood perfusion and then reduced it to 12.5 cmH_2O (9.2 mmHg = 1.2 kPa) for 3 min of saline/dextran perfusion followed by intravascular fixation at the same pressure. The results showed that ~70% of both the endothelial and epithelial breaks closed within that short period of time. It was also found that most of the breaks that closed were those that were initially small, and those associated with an intact basement membrane.

F. Possible Micromechanics of Stress Failure

Very little is known about the micromechanics of the ultrastructural changes described above. One important clue may be the rapid reversibility of many of the disruptions when the capillary transmural pressure was reduced. This suggests that there is an elastic component to the process, elasticity being defined as the tendency of a distorted structure to return to its original configuration when the distorting stress is removed. One possibility is that the basement membrane scaffolding is elongated in the direction of the applied stress. As indicated earlier, type IV collagen molecules are assembled into a matrix configuration rather like chicken wire (Fig. 15). As also mentioned above, type IV collagen molecules have bending sites that may allow the matrix to distort. Figure 20 shows how the matrix configuration might be elongated rather as occurs when chicken wire is pulled in one direction. If the overlying cells are not able to elongate to the same extent, intracellular disruptions might be inevitable.

A feature of the electron micrographs shown in Figure 19 is that the disrupted ends of the cells can be far apart while the basement membrane remains intact. This is clearly shown in Figure 19*A* for a capillary endothelial cell, and even more strikingly in Figure 19*B* where near the top of the micrograph the ends of the disrupted alveolar epithelial cell are separated by ~6 μm. These appear-

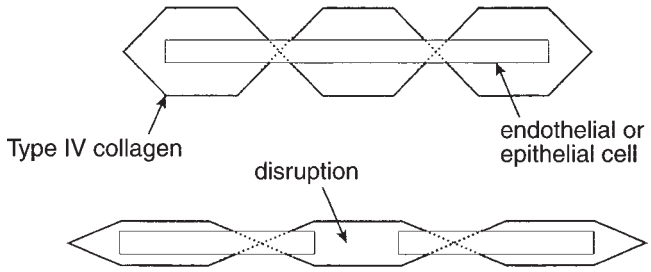

FIG. 20. Diagram to show how distortion of the type IV collagen matrix shown in Figure 1 might cause disruptions in the capillary endothelial or alveolar epithelial layers. *A*: the normal situation at a low capillary transmural pressure. *B*: the results of distorting the matrix. [Modified from West and Mathieu-Costello (251).]

ances raise the question of whether the cells can move along the basement membrane by detaching and reattaching the links, for example, via integrins. It is certainly accepted that cells migrate along basement membranes during development. It is also known that some interactions between cells and underlying structures can cycle on and off at very rapid rates. One example is the attachments between leukocytes and capillary endothelial cells that allow leukocytes to roll along an endothelial surface. Calculations show that the points of attachment between the leukocytes and the underlying epithelial cells must break and connect many times a second to allow this behavior to occur (79). Therefore, it seems possible that attachments formed by integrins or other molecules between the overlying endothelial or epithelial cells and their basement membranes are able to break and make rapidly.

Another interesting question is how does the cell wall reconstitute itself after an intracellular disruption? Presumably the mechanism is the same one that allows the bilipid layer to reestablish its normal structure after the cell surface has been disrupted by an emerging pinocytotic vesicle. The bilipid layer that makes up the cell membrane has an intrinsic stability and tendency to reconfigure. Sometimes people have questioned whether an intracellular disruption will result in spilling out of some of the contents of the cell, but here it should be remembered that the cell is highly compartmentalized by the cytoskeleton and other organelles, and the cytoplasm itself rapidly fluxes from sol to gel states depending on prevailing environmental conditions.

G. Physiological Conditions Under Which Stress Failure Occurs

It might be concluded from the above, and particularly the electron micrographs shown in Figure 19, that stress failure of pulmonary capillaries is a grossly pathological condition and hardly material for a physiological review. However, it is now clear that stress failure of pulmonary capillaries occurs under physiological conditions. The best example of this is so-called exercise-induced pulmonary hemorrhage, which commonly occurs in racehorses (185) and possibly in normal resting birds (178).

It has been known since Elizabethan times that some racehorses have blood issuing from their nostrils after galloping (horses are obligate nose breathers and cannot breathe through their mouths because they cannot raise their remarkably long soft palate high enough to open the air passage). For many years it was thought that this bleeding was very unusual and it was ascribed to all sorts of exotic hazards such as moldy hay, a condition commonly termed guttural pouch mycosis. However, when veterinarians became more interested in the problem, they started bronchoscoping horses after races and showed that ~70% of Thoroughbreds had frank blood visible in their bronchi after racing (185). Finally, Whitwell and Greet (254) collected tracheal washings from racehorses and showed that 100% of Thoroughbreds in training had hemosiderin-laden macrophages in their lung. The inescapable conclusion was that all Thoroughbred racehorses in training bleed into their lungs, surely an extraordinary finding.

The reason for the bleeding became clear when the pulmonary vascular pressures of Thoroughbreds were measured while they were galloping on a treadmill (61, 112). Direct measurements showed left atrial pressures as high as 70 mmHg (9.3 kPa) and pulmonary artery pressures as high as 120 mmHg (16 kPa). Other vascular pressures are equally astonishing with a mean systemic arterial pressures as high as 240 mmHg (32 kPa) and a mean right atrial pressure of 40 mmHg (5.3 kPa). The basic reason for these remarkable pressures is that these animals have been selectively bred for hundreds of years for extremely high aerobic performances. Maximal oxygen consumptions of up to 180 ml $\cdot$ min^{-1} $\cdot$ kg^{-1} and cardiac outputs as high as 750 ml $\cdot$ min^{-1} $\cdot$ kg^{-1} have been reported. These enormous cardiac outputs require very high filling pressures in the left ventricle, and therefore very high left atrial and pulmonary venous pressures. Incidentally, there is no evidence of an increased pulmonary vascular resistance; the pulmonary artery pressure is only raised in response to the increased pulmonary venous pressures. It follows that during galloping the pressure in the pulmonary capillaries must be of the order of 100 mmHg (13.3 kPa), and of course it is not surprising that stress failure occurs under these conditions. Indeed, it would be astonishing if it did not. We have been able to demonstrate breaks in the blood-gas barrier of Thoroughbreds after they have galloped on a treadmill (252).

It might be argued that this finding of stress failure of pulmonary capillaries is a physiological oddity in that these animals are monsters because of a long history of

selective breeding. However, there is also evidence that elite human athletes during maximal exercise have changes in the integrity of the blood-gas barrier. Hopkins et al. (98) persuaded six elite cyclists to sprint uphill at maximal effort sufficient to give a mean heart rate of 177 beats/min and then undergo bronchoalveolar lavage (BAL) within an hour of finishing the exercise. The results were compared with those from normal sedentary volunteers who did not exercise before BAL. It was found that the athletes had significantly higher concentrations of red blood cells, total protein, albumin, and leukotriene B_4 (LTB_4) in their BAL fluid than control subjects. It seems inescapable that brief but very intense exercise in these elite athletes caused changes in the structure of the blood-gas barrier. The result is consistent with other anecdotal reports of bleeding in swimmers and runners following very severe exercise (164, 242).

An interesting question is whether more prolonged but submaximal exercise causes similar changes in the blood-gas barrier. To test this Hopkins et al. (97) carried out an additional study on another group of six elite cyclists who exercised at 77% of their maximal oxygen consumption for 1 h before undergoing BAL. Again, the controls were normal nonathletes who did not exercise before BAL. In contrast to the results of the previous study, the concentrations of red blood cells, total protein, and LTB_4 in the BAL fluid of the exercising athletes were not different from those of the control subjects. There were higher concentrations of surfactant apoprotein A in the athletes, but this is known to occur with exercise (50). The general conclusion of these studies is that the integrity of the blood-gas barrier in normal healthy humans is altered only at extreme levels of exercise, and indeed this is what might be expected on general evolutionary lines.

H. Pathological Conditions Leading to Stress Failure

Since normal subjects develop changes in the integrity of their pulmonary capillaries at very high but nevertheless physiological pressures, it is not surprising that pathological conditions that raise the transmural pressure of the capillaries to unphysiologically high levels will cause stress failure (248). This topic will only be treated very briefly here because the emphasis of this review is on normal physiology. Pathological conditions in which high capillary pressures cause a high-permeability type of edema indicating damage to the capillary wall include high-altitude pulmonary edema briefly referred to earlier, and neurogenic pulmonary edema which sometimes follows head trauma. Both alveolar edema and hemorrhage are seen when the pulmonary capillary pressure is raised to abnormally high levels by cardiac diseases such as left ventricular failure or mitral stenosis. A particularly interesting situation is that caused by abnormally high states of lung inflation as sometimes seen, for example, during mechanical ventilation in the intensive care unit. It has been known for many years that damage to the pulmonary capillaries occurs with high levels of positive end-expiratory pressure which result in large lung volumes. Here the mechanism of the stress failure is the increased longitudinal tension in the alveolar wall, shown as mechanism number 2 in Figure 18. Recent studies suggest that using smaller tidal volumes during mechanical ventilation in these patients results in less damage to the capillaries (28), although the area is somewhat controversial. Finally, patients with Goodpasture's syndrome develop stress failure of their pulmonary capillaries as briefly referred to earlier. The reason is that an antibody attacks the NC1 globular domain of type IV collagen (256) presumably affecting its strength and bleeding occurs into both the alveolar and glomerular spaces.

I. Regulation of the Blood-Gas Barrier in Response to Wall Stress

As has been emphasized throughout this review, the blood-gas barrier has a dilemma in that it is required to be extremely thin for efficient gas exchange, but it must also be immensely strong because of the stresses that develop as a result of its thinness. A basic biological question is how the blood-gas barrier is maintained so exquisitely thin but just strong enough to withstand all but the most extreme physiological stresses. Or to put it another way, how is the structure of the blood-gas barrier regulated to optimize these conflicting requirements. The most likely hypothesis is that the capillary wall senses wall stress in some way, and as a result its structure, presumably particularly the amount of type IV collagen in the extracellular matrix, is adjusted accordingly.

It is well-known that remodeling of the structure of larger pulmonary blood vessels frequently occurs in response to increased stress. An example is the hypertrophy of smooth muscle and other structures in the walls of pulmonary arteries that occurs when animals are placed in a hypoxic environment, and the pulmonary artery pressure rises as a result of hypoxic pulmonary vasoconstriction. There is a large amount of literature on pulmonary vascular remodeling with extensive reviews, for example, Stenmark and Mecham (212). In contrast, remodeling of pulmonary capillaries in response to increased capillary pressure has been almost completely ignored, although we know it occurs because, for example, patients with mitral stenosis whose pulmonary capillary pressures are raised over months or years show marked thickening of the capillary wall basement membranes (93).

A number of experiments have been carried out in our laboratory over the last few years to elucidate the

mechanism of remodeling of pulmonary capillaries, but these will not be described in detail here. Suffice it to say that various studies where the capillary wall stress has been increased by raising the transmural pressure, or increasing lung volume (see Fig. 18), have shown increases in mRNA for procollagens α1(I), α2(II), and α2(IV), fibronectin, laminin, basic fibroblast growth factor, TGF-β1, and platelet-derived growth factor B (11, 12, 182). Other experiments have shown calcium ion dependence of mechanical injury to the capillaries (184), and also that gadolinium apparently protects capillaries against stress failure caused by high lung volumes (183). More work is needed on this central problem in lung cell and molecular biology.

IV. CONCLUDING REMARKS: COMPROMISE DESIGN OF THE BLOOD-GAS BARRIER

Molecular oxygen is vital for generation of energy that in turn is fundamental to life. For that matter, nature has been particularly inventive in the designs of the respiratory organs. The many cases of convergence and conservation of respiratory structures, e.g., the three-ply design of the blood-gas barrier and the biochemistry of the surfactant, are examples of ardent pursuit for optimal solutions to needs for molecular oxygen. In the midst of remarkable structural heterogeneity of the external morphologies of the gas exchangers, features determined by factors such as body size, life-style, phylogeny, and habitat occupied, essentially comprising thin epithelial and endothelial cells that are coupled by intercellular matrix, at the level of the water/blood-gas barrier, a shared architecture (a three-ply design) exists.

The three-ply design of the water/blood-gas barrier appeared very early in the evolution of the vertebrate gas exchanger. Although less conspicuously, it exists in the gills of ancient fish like the coelacanth, *Latimeria chalumnae*, and those of the modern teleost species and in the lungs of the highly conserved lungfishes (Dipnoi) to those of the contemporary air-breathing vertebrates. Occurring both spatially (i.e., across diverse animal taxa) and temporally (i.e., along the evolutionary time), in all probability, the architecture of the water/blood-gas barrier has been preserved for its optimal functional and structural properties. Thinness of the water/blood-gas barrier was essential for efficient gas exchange by passive diffusion, while strength was necessary for maintenance of structural integrity. Unquestionably, the conflicting functional requirements presented formidable bioengineering challenges. Trade-offs and compromises were necessary in overcoming the limitations that were central to the inauguration of the three-ply design. There is persuasive evidence that type IV collagen in the lamina densa of the basement membrane of the extracellular matrix of the blood-gas barrier is the chief component with the highest ultimate tensile strength. Under extreme conditions/states of operation, the barrier fails with dire consequences. Further investigations are necessary on the respiratory organs/structures of different animal groups to comprehensively understand the biomechanics of the water/blood-gas barrier, especially from adaptive and phylogenetic perspectives.

This work was supported by National Heart, Lung, and Blood Institute Grant RO1-HL-60698. J. N. Maina's recent studies have been funded by the University of the Witwatersrand Research Committee and Faculty of Health Sciences of the University of the Witwatersrand Research Endowment Grants.

Address for reprint requests and other correspondence: J. B. West, UCSD Department of Medicine 0623A, 9500 Gilman Dr., La Jolla, CA 92093-0623 (E-mail: jwest@ucsd.edu).

REFERENCES

1. **Abdalla MA and Maina JN.** Quantitative analysis of the exchange tissue of the avian lung (*Galliformes*). *J Anat* 134: 677–680, 1981.
2. **Abdalla MA, Maina JN, King AS, King DZ, and Henry J.** Morphometrics of the avian lung. 1. The domestic fowl, *Gallus domesticus*. *Respir Physiol* 47: 267–278, 1982.
3. **Alexander McN.** Symmorphosis and safety factors. In: *Principles of Animal Design: The Optimization and Symmorphosis Debate*, edited by Weibel ER, Taylor CR, and Bolis L. Cambridge, UK: Cambridge Univ. Press, 1998, p. 28–35.
4. **Andrews P.** Characteristic surface topographies of cells lining the respiratory tract. *Biomed Res* 2: 281–288, 1981.
5. **Aschopf J and Pohl H.** Rhythmic variations in energy metabolism. *Federation Proc* 29: 1541–1552, 1970.
6. **Atwal OS, Sigh B, Staempfli H, and Minhas KJ.** Presence of pulmonary intravascular macrophages in the equine lung: some structuro-functional properties. *Anat Rec* 234: 530–540, 1992.

6a. **Bachofen H, Schürch S, Urbinelli M, and Weibel ER.** Relations among alveolar surface tension, surface area, volume, and recoil pressure. *J Appl Physiol* 62: 1878–1887, 1987.

7. **Bakhle YS and Vane JR**(Editors). *Metabolic Functions of the Lung*. New York: Dekker, 1977.
8. **Barker FK, Cibois A, Schikler P, Fenstein J, and Cracraft J.** Phylogeny and diversification of the largest avian radiation. *Proc Natl Acad Sci USA* 101: 11040–11045, 2004.
9. **Becker KL.** The endocrine lung. In: *The Endocrine Lung in Health and Disease*, edited by Becker KL and Gadzar AF. Philadelphia, PA: Saunders, 1984, p. 3–46.
10. **Bemis WE, Burggren WW, and Kemp NE**(Editors). *The Biology and Evolution of Lungfishes*. New York: Liss, 1987.
11. **Berg JT, Breen EC, Fu Z, Mathieu-Costello O, and West JB.** Alveolar hypoxia increases gene expression of extracellular matrix proteins and platelet-derived growth factor-B in lung parenchyma. *Am J Respir Crit Care Med* 158: 1920–1928, 1998.
12. **Berg JT, Fu Z, Breen EC, Tran HC, Mathieu-Costello O, and West JB.** High lung inflation increases mRNA levels of ECM components and growth factors in lung parenchyma. *J Appl Physiol* 83: 120–128, 1997.
13. **Bettex-Galland M and Hughes GM.** Contractile filamentous material in the pillar cells of fish gills. *J Cell Sci* 13: 359–366, 1973.
14. **Bhattacharya J and Staub NC.** Direct measurement of microvascular pressures in the isolated perfused dog lung. *Science* 210: 327–328, 1980.
15. **Bils RF and Hughes GM.** Inner surface ultrastructure of the lungs of the frog and lizard. *9th Int Cong Electron Microsc 9th Toronto Canada 1978*, vol. II.
16. **Birks EK, Mathieu-Costello O, Fu Z, Tyler WS, and West JB.** Comparative aspects of the strength of pulmonary capillaries in rabbit, dog, and horse. *Respir Physiol* 97: 235–246, 1994.

17. **Birks EK, Mathieu-Costello O, Fu Z, Tyler WS, and West JB.** Very high pressures are required to cause stress failure of pulmonary capillaries in Thoroughbred racehorses. *J Appl Physiol* 82: 1584–1592, 1997.
18. **Blumberg B, MacKrell AJ, and Fessler JH.** *Drosophila* basement membrane procollagen alpha 1(IV). II. Complete cDNA sequence, genomic structure, and general implications for supramolecular assemblies. *J Biol Chem* 263: 18328–18337, 1988.
19. **Bohr C.** über die spezifische Tätigkeit der Lungen bei der respiratorischen Gasaufnahme. *Scand Arch Physiol* 22: 221–280, 1909.
20. **Bourbon JR and Chailley-Heu B.** Surfactant proteins in the digestive tract, mesentery, and other organs: evolutionary significance. *Comp Biochem Physiol A Mol Integr Physiol* 129: 151–161, 2001.
21. **Bowden DH.** Macrophages, dust, and pulmonary diseases. *Exp Lung Res* 12: 89–107, 1987.
22. **Brain JD and Hyg SD.** Lung macrophages: how many kinds are there: what do they do? *Am Rev Respir Dis* 137: 507–509, 1988.
23. **Rain JD, Proctor DF, and Reid LM**(Editors). *Respiratory Defense Mechanisms*, *Part I.* New York: Dekker, 1977.
24. **Brain JD, Proctor DF, and Reid LM**(Editors). *Respiratory Defense Mechanisms*, *Part II.* New York: Dekker, 1977.
25. **Breeze RG and Wheeldon EB.** The cells of the pulmonary airways. *Am Rev Respir Dis* 116: 705–777, 1977.
26. **Brenner BM and Humes HD.** Mechanics of glomerular ultrafiltration. *N Engl J Med* 297: 148–154, 1977.
27. **Brinkman H, Venkatesh B, Brenner S, and Meyer A.** Nuclear protein-coding genes support lungfish and not the coelacanth as the closest living relatives of land vertebrates. *Proc Natl Acad Sci USA* 101: 4900–4905, 2004.
28. **Brower RG, Matthay MA, Morris A, Schoenfeld D, Thompson BT, and Wheeler A.** Ventilation with lower tidal volumes compared with traditional tidal volumes for acute lung injury and the acute respiratory distress syndrome. *N Engl J Med* 342: 1301–1308, 2000.
29. **Burri PH.** Morphology and respiratory function of the alveolar unit. *Int Archs Allergy Appl Immunol* 76: 2–12, 1985.
30. **Butler PJ and Metcalfe JD.** Control of respiration and circulation. In: *Control Processes in Fish Physiology,* edited by Rankin RC, Pitcher TJ, and Duggan RJ. Beckenham: Croom Helm, 1983, p. 41–65.
31. **Campbell H and Tomkeief SI.** Calculation of internal surface area of a lung. *Nature* 170: 117, 1952.
32. **Campbell NA, Reece JB, and Simon EJ.** *Essential Biology.* San Francisco, CA: Pearson, 2004.
33. **Cardodo WV.** Molecular regulation of lung development. *Annu Rev Physiol* 63: 471–494, 2001.
34. **Chalkley HW.** Method for the quantitative analysis of tissues. *J Nat Cancer Inst* 4: 47–53, 1943.
35. **Chapman DJ and Schopf JW.** *Biological* and biochemical effects of the development of an aerobic environment. In: *Earth's Earliest Biosphere: Its Origin and Evolution*, edited by Schopf JW. Princeton, NJ: Princeton Univ. Press, 1983, p. 302–320.
36. **Codd Slocombe NC, Daniels CB, Wood PG Jr, and Orgeig S.** Periodic fluctuations in the pulmonary surfactant system in Gould's wattled bat (*Chalinolobus gouldii*). *Physiol Biochem Zool* 73: 605–612, 2000.
37. **Costello ML, Mathieu-Costello O, and West JB.** Stress failure of alveolar epithelial cells studied by scanning electron microscopy. *Am Rev Respir Dis* 145: 1446–1455, 1992.
38. **Cragg P.** *Respiration and Body Weight in the Reptilian Genus Lacerta: A Physiological, Anatomical and Morphometric Study* (PhD thesis). Bristol, UK: Univ. of Bristol, 1975.
39. **Crapo JD, Barry BE, Gehr P, Bachofen M, and Weibel ER.** Cell number and cell characteristics of the normal human lung. *Am Rev Respir Dis* 126: 332–337, 1982.
40. **Crapo JD, Young SL, Fram EK, Pinkerton KE, Barry BE, and Crapo RO.** Morphogenetic characteristics of cells in the alveolar region of mammalian lungs. *Am Rev Respir Dis* 128: S42–S46, 1983.
41. **Crouch EC, Martin GR, Jerome BS, and Laurie GW.** Basement membranes. In: *The Lung: Scientific Foundations*, edited by Crystal RG, West JB, Weibel ER, and Barnes PJ. Philadelphia, PA: Lippincott-Raven, 1997, vol. I, p. 769–791.
42. **Crowell RE, Heaphy E, Valdez YE, Mold C, and Lehnert BE.** Alveolar and interstitial macrophage populations in the murine lung. *Exp Lung Res* 18: 435–446, 1992.
43. **Czopek J.** Smooth muscle in the lungs of some urodeles. *Nature* 193: 798–811, 1962.
44. **Czopek J.** Vascularization of respiratory surfaces in some Caudates. *Copeia* 1962: 576–587, 1962.
45. **Czopek J.** Quantitative studies of the morphology of respiratory surfaces in amphibians. *Acta Anat* 62: 296–323, 1965.
46. **Daniels CB, Orgeig S, Wilsen J, and Nicholas TE.** Pulmonary-type surfactants in the lungs of terrestrial and aquatic amphibians. *Respir Physiol* 95: 249–258, 1994.
47. **Defouw DO.** Vesicle numerical densities and cellular attenuation: comparisons between endothelium and epithelium of the alveolar septa in normal dog lungs. *Anat Rec* 209: 77–84, 1984.
48. **Dock DS, Kraus WL, McGuire LB, Hyland JW, Haynes FW, and Dexter L.** The pulmonary blood volume in man. *J Clin Invest* 40: 317–328, 1961.
49. **Dormans JA.** The alveolar type III cell. *Lung* 163: 327–335, 1985.
50. **Doyle IR, Jones ME, Barr HA, Orgeig S, Crockett AJ, McDonald CF, and Nicholas TE.** Composition of human pulmonary surfactant varies with exercise and level of fitness. *Am J Respir Crit Care Med* 149: 1619–1627, 1994.
51. **Dubach M.** Quantitative analysis of the respiratory system of the house sparrow, budgerigar, and violet-eared hummingbird. *Respir Physiol* 46: 43–60, 1981.
52. **Duncker HR and Guntert M.** The quantitative design of the avian respiratory system: from hummingbird to the mute swan. In: *BIONA Report No. 3*, edited by Nachtigall W. Stuttgart, Germany: Gustav-Fischer Verlag, 1985, p. 361–378.
53. **Duncker HR and Guntert M.** Morphometric analysis of the avian respiratory system. In: *Vertebrate Morphology*, edited by Duncker HR and Fleischer G. Stuttgart, Germany: Gustav-Fischer, 1985, p. 383–387.
54. **Dunnill MS.** Quantitative methods in the study of pulmonary morphology. *Thorax* 17: 320–328, 1962.
55. **Dunnill MS.** Evaluation of a simple method of sampling the lung for quantitative histological analysis. *Thorax* 19: 443–448, 1964.
56. **Dunnill MS.** Effect of lung inflation on alveolar surface area in the dog. *Nature* 214: 1013–1015, 1967.
57. **Effros RM, Mason GR, Silverman P, Reid E, and Hukkanen J.** Movement of ions and small solutes across endothelium and epithelium of perfused rabbit lungs. *J Appl Physiol* 60: 100–107, 1986.
58. **Ekelund LG and Holmgren A.** Central hemodynamics during exercise. *Circ Res* 30 *Suppl* I: I33–I43, 1967.
59. **Elliott AR, Fu Z, Tsukimoto K, Prediletto R, Mathieu-Costello O, and West JB.** Short-term reversibility of ultrastructural changes in pulmonary capillaries caused by stress failure. *J Appl Physiol* 73: 1150–1158, 1992.
60. **Engel J, Odermatt E, Engel A, Madri JA, Furthmayr H, Rohde H, and Timpl R.** Shapes, domain organizations and flexibility of laminin and fibronectin, two multifunctional proteins of the extracellular matrix. *J Mol Biol* 150: 97–120, 1981.
61. **Erickson BK, Erickson HH, and Coffman JR.** Pulmonary artery and aortic pressure changes during high intensity treadmill exercise in the horse: effect of furosemide and phentolamine. *Equine Vet J* 24: 215–219, 1992.
62. **Fisher RF and Wakely J.** The elastic constants and ultrastructural organization of a basement membrane (lens capsule). *Proc R Soc Lond B Biol Sci* 193: 335–358, 1976.
63. **Fishman AP.** Pulmonary edema; the water-exchanging function of the lung. *Circulation* 46: 390–408, 1972.
64. **Fishman AP and Fisher AB**(Editors). *Handbook of Physiology. The Respiratory System. Circulation and Nonrespiratory Functions.* Bethesda, MD: Am. Physiol. Soc., 1985, sect. 3, vol. I.
65. **Fons R and Sicart R.** Contribution à la connaissance du métabolisme énergétique chez deux Crocidurinae: *Suncus etruscus* (Savi 1822) et *Crocidura russula* (Herman 1780), Insectivora, Soricidae, Mammalia. *Mammalia* 40: 229–311, 1976.
66. **Forrest JB.** The effect of changes in lung volume in the size and shape of the alveoli. *J Physiol* 210: 533–549, 1970.
67. **Forster RE.** Transfer of gas by diffusion and chemical reaction in pulmonary capillaries. In: *Respiration Physiology: Peoples and*

Ideas, edited by West JB. New York: Oxford Univ. Press, 1996, p. 49–74.
68. **Fu Z, Costello ML, Tsukimoto K, Prediletto R, Elliot AR, Mathieu-Costello O, and West JB.** High lung volume increases stress failure in pulmonary capillaries. *J Appl Physiol* 73: 123–133, 1992.
69. **Fu Z, Heldt G, and West JB.** Increased fragility of pulmonary capillaries in newborn rabbit. *Am J Physiol Lung Cell Mol Physiol* 284: L703–L709, 2003.
70. **Fu Z, Heldt GP, and West JB.** Thickness of the blood-gas barrier in premature and 1 day old newborn rabbit lungs. *Am J Physiol Lung Cell Mol Physiol* 285: L130–L136, 2003.
71. **Fung YC.** *Biomechanics: Mechanical Properties of Living Tissues* (2nd ed.). New York: Springer-Verlag, 1993.
72. **Fung YC and Sobin SS.** Theory of sheet flow in lung alveoli. *J Appl Physiol* 26: 472–488, 1969.
73. **Gannon BJ, Campbell G, and Randall DJ.** Scanning electron microscopy of vascular casts for the study of vessel connections in a complex vascular bed–the trout gill. *Proc Elect Microsc Soc Am* 31: 442–443, 1973.
74. **Gehr P, Bachofen M, and Weibel ER.** The normal human lung: ultrastructure and morphometric estimation of diffusion capacity. *Respir Physiol* 32: 121–140, 1978.
75. **Gehr P, Mwangi DK, Amman A, Maloiy GMO, Taylor CR, and Weibel ER.** Design of the mammalian respiratory system. V. Scaling morphometric pulmonary diffusing capacity to body mass: wild and domestic animals. *Respir Physiol* 44: 61–86, 1981.
76. **Gehr P, Sehovic S, Burri PH, Claasen H, and Weibel ER.** The lung of shrews: morphometric estimation of diffusion capacity. *Respir Physiol* 44: 61–86, 1980.
77. **Glazier JB, Hughes JM, Maloney JE, and West JB.** Measurements of capillary dimensions and blood volume in rapidly frozen lungs. *J Appl Physiol* 26: 65–76, 1969.
78. **Goerke J.** Pulmonary surfactant: functions and molecular composition. *Biochim Biophys Acta* 1408: 79–89, 1998.
79. **Goetz Dj, el-Sabban ME, Pauli BU, and Hammer DA.** Dynamics of neutrophil rolling over stimulated endothelium in vitro. *Biophys J* 66: 2202–2209, 1994.
80. **Goldie RG, Bertram JF, Warton A, Papadimitriou JM, and Paterson JW.** Pharmacological and ultrastructural study of alveolar contractile tissue in toad (*Bufo marinus*) lung. *Comp Biochem Physiol* 75: 343–349, 1983.
81. **Goniakowska-Witalinska L.** Ultrastructure and morphometric study of the lung of the European salamander, *Salamandra salamandra* L. *Cell Tissue Res* 191: 43–356, 1978.
82. **Goniakowska-Witalinska L.** Ultrastructural and morphometric changes in the lung of newt, *Triturus cistatus carnifex* (Laur. *)* during ontogeny. *J Anat* 130: 571–583, 1980.
83. **Goniakowska-Witalinska L.** Scanning and transmission electron microscopic study of the lung of the newt, *Triturus alpestris* Laur. *Cell Tissue Res* 205: 133–145, 1980.
84. **Goniakowska-Witalinska L and Leuweryns JM.** Brush cells in the lungs of *Bombina orientalis* (Boul) (Anura, Amphibia). *J Submicrosc Pathol* 23: 123–130, 1991.
85. **Goniakowska-Witalinska L.** The histology and ultrastructure of the amphibian lung. In: *Histology, Ultrastructure and Immunohistochemistry of the Respiratory Organs in Non-Mammalian Vertebrates*, edited by Pastor LM. Murcia, Spain: Publicaciones Universidad de Murcia, 1995, p. 77–112.
86. **Graham JB, Dudley R, Aguillar NM, and Gans C.** Implications of the late Paleozoic oxygen pulse for physiology and evolution. *Nature* 375: 117–120, 1995.
87. **Grant MM, Brain JD, and Vinegar A.** Pulmonary defense mechanisms in *Boa constrictor*. *J Appl Physiol* 50: 979–983, 1981.
88. **Grote J.** Die Sauerstoffdiffusionskonstanten im Lungengewebe und Wasser und ihre Temperaturabhängigkeit. *Pflügers Arch* 295: 245–254, 1967.
89. **Groves BM, Reeves JT, Sutton Wagner PD, Cymerman A Jr, Malconian MK, Rock PB, Young PM, and Houston CS.** Operation Everest II: elevated high-altitude pulmonary resistance unresponsive to oxygen. *J Appl Physiol* 63: 521–530, 1987.
90. **Gundersen HJG, Jensen TB, and Østerby R.** Distribution of membrane thickness determined by lineal analysis. *J Microsc* 113: 27–43, 1978.
91. **Haldane JS and Priestley JG.** *Respiration.* London: Oxford Univ. Press, 1935.
92. **Hartwell LH, Hopfield JJ, Leiber S, and Murray AW.** From molecular to modular cell biology. *Nature* 40: 47–52, 1999.
93. **Haworth SG, Hall SM, and Patel M.** Peripheral pulmonary vascular and airway abnormalities in adolescents with rheumatic mitral stenosis. *Int J Cardiol* 18: 405–416, 1988.
94. **Henk WG and Haldman JT.** Microanatomy of the lung of the bowhead whale *Balaena mysticetus*. *Anat Rec* 226: 187–197, 1990.
95. **Hennig A.** A critical survey of volume and surface measurements in microscopy. *Zeiss Werkzeitschrift* 30: 78–87, 1959.
96. **Hoffman H, Voss T, Kukn K, and Engel J.** Localization of flexible sites in thread-like molecules from electron micrographs. Comparison of interstitial, basement membrane and intima collagens. *J Mol Biol* 172: 325–343, 1984.
97. **Hopkins SR, Schoene RB, Henderson WR, Spragg RG, and West JB.** Sustained submaximal exercise does not alter the integrity of the lung blood-gas barrier in elite athletes. *J Appl Physiol* 84: 1185–1189, 1998.
98. **Hopkins SR, Schoene RB, Martin TR, Henderson WR, Spragg RG, and West JB.** Intense exercise impairs the integrity of the pulmonary blood-gas barrier in elite athletes. *Am J Respir Crit Care Med* 155: 1090–1094, 1997.
99. **Houlihan DF, Rankin JC, and Shutleworth TJ**(Editors). *Gills*. Cambridge, UK: Cambridge Univ. Press, 1982.
100. **Hughes GM.** The dimensions of fish gills in relation to their function. *J Exp Biol* 45: 177–195, 1966.
101. **Hughes GM.** Fish respiratory physiology. In: *Perspectives in Environmental Biology*, edited by Spencer-Davies P. Oxford, UK: Pergamon, 1976, p. 235–245.
102. **Hughes GM.** Ultrastructure and morphometry of the gills of *Latimeria chalumnae* and a comparison with the gills of associated fishes. *Proc R Soc Lond B Biol Sci* 208: 309–328, 1980.
103. **Hughes GM.** The gills of the coelacanth, *Latimeria chalumnae*, a study in relation to body size. *Phil Trans R Soc Lond B Biol Sci* 347: 427–438, 1995.
104. **Hughes GM and Grimstone AV.** The fine structure of the secondary lamellae of the gills of *Gadus pollachius*. *Q J Microsc Sci* 106: 343–353, 1965.
105. **Hughes GM and Morgan M.** The structure of fish gills in relation to their respiratory function. *Biol Rev* 48: 419–475, 1973.
106. **Hughes GM and Mittal AK.** Structure of the gills of *Barbus sophor* (Ham), a cyprinid with tertiary lamellae. *J Fish Biol* 16: 461–467, 1980.
107. **Hughes GM and Munshi JSD.** Fine structure of the respiratory surfaces of an air breathing fish, the climbing perch, *Anabas testudineus*. *Nature* 219: 1382–1384, 1968.
108. **Hughes GM and Weibel ER.** Morphometry of fish lungs. In: *Respiration of Amphibious Vertebrates*, edited by Hughes GM. London: Academic, 1976, p. 213–232.
109. **Hughes GM and Weibel ER.** Visualization of layers lining the lung of the South American lungfish, *Lepidosiren paradoxa* and a comparison with the frog and the rat. *Tissue Cell* 10: 343–353, 1978.
110. **Hughes GM and Wright DE.** A comparative study of the ultrastructure of the water/blood pathway in the secondary lamellae of teleost and elasmobranch fishes—benthic forms. *Z Zellforsch Mikrosk Anat* 104: 478–493, 1970.
111. **Jones JH, Effman EL, and Schmidt-Nielsen K.** Lung volume changes during respiration in ducks. *Respir Physiol* 59: 15–25, 1985.
112. **Jones JH, Smith BL, Birks EK, Pascoe JR, and Hughes TR.** Left atrial and pulmonary artery pressures in exercising horses (Abstract). *FASEB J* 6: A202, 1992.
113. **Junod AE and de Haller R** (Editors). *Lung Metabolism*. New York: Academic, 1975.
114. **Kern A, Eble J, Golbik R, and Kühn K.** Interaction of type IV collagen with the isolated integrins a1b1 and a2b1. *Eur J Biochem* 215: 151–159, 1993.

115. **Kleinman HK, Cannon FB, Laurie GW, Hassell JR, Aumailley M, Terranova VP, Martin GR, and DuBOIS-Dalcq M.** Biological activities of laminin. *J Cell Biochem* 27: 317–325, 1985.
116. **Klika E, Scheuermann DW, De Groodt-Lasseel MHA, Bazantova I, and Switka A.** Pulmonary macrophages in birds (barn owl, *Tyto tyto alba*), domestic fowl (*Gallus gallus domestica*), quail (*Coturnix coturnix*), and pigeons (*Columba livia*). *Anat Rec* 256: 87–97, 1996.
117. **Klika E, Scheuermann DW, De Groodt-Lasseel MHA, Bazantova I, and Switka A.** Anchoring and support system of pulmonary gas exchange tissue in four bird species. *Acta Anat* 159: 30–41, 1997.
118. **Klingele TG and Staub NC.** Alveolar shape changes with volume in isolated, air filled lobes of cat lung. *J Appl Physiol* 28: 411–423, 1965.
119. **Kuno K and Staub NC.** Acute mechanical effects of lung volume changes on artificial microholes in alveolar walls. *J Appl Physiol* 24: 83–98, 1968.
120. **Lasiewski RC and Dawson WR.** A re-examination of the relation between standard metabolic rate and body weight in birds. *Condor* 69: 13–23, 1967.
121. **Laurent P.** Structure of vertebrate gills. In: *Gills*, edited by Houlihan DF, Rankin JC, and Shuttleworth TJ. Cambridge, UK: Cambridge Univ. Press, 1982, p. 25–43.
122. **Laurent P, Maina JN, Wood CM, Walsh PJ, Bergman HL, and Narahara AB.** The morphology of the gills of *Oreochromis alcalicus grahami* a fish that lives in an alkaline pH water. *Can J Zool* 73: 1170–1181, 1995.
123. **Leblond CP and Inoue S.** Structure, composition, and assembly of basement membrane. *Am J Anat* 185: 367–390, 1989.
124. **López J.** Anatomy and histology of the lung and air sacs of birds. In: *Histology, Ultrastructure and Immunohistochemistry of the Respiratory Organs in Non-Mammalian Vertebrates*, edited by Pastor LM. Murcia, Spain: Publicaciones de la Universitatd de University of Murcia, 1995, p. 179–233.
125. **Luchtel DL and Kardong KV.** Ultrastructure of the lung of the rattlesnake, *Crotalus viridis oreganus*. *J Morphol* 169: 29–47, 1981.
126. **Maarek JMI and Chang HK.** Pulsatile pulmonary microvascular pressure measured with vascular occlusion techniques. *J Appl Physiol* 70: 998–1005, 1991.
127. **Maina JN.** Morphometrics of the avian lung. 3. The structural design of the passerine lung. *Respir Physiol* 55: 291–309, 1984.
128. **Maina JN.** The morphology of the lung of the African lungfish, *Protopterus aethiopicus*: a scanning electron microscopic study. *Cell Tissue Res* 250: 191–196, 1987.
129. **Maina JN.** Morphometrics of the avian lung. 4. The structural design of the charadriiform lung. *Respir Physiol* 68: 99–119, 1987.
130. **Maina JN.** The morphology and morphometry of the adult normal baboon lung *Papio anubis*. *J Anat* 150: 29–246, 1987.
130a. **Maina JN.** The morphology and morphometry of the normal lung of the adult vervet monkey *Cereopithecus acthiops*. *Am J Anat* 183: 258–267, 1988.
131. **Maina JN.** The morphology of the lung of the East African tree frog *Chiromantis petersi* with observations on the skin and the buccal cavity as secondary gas exchange organs: A TEM and SEM study. *J Anat* 165: 29–43, 1989.
132. **Maina JN.** The morphometry of the avian lung. In: *Form and Function in Birds*, edited by King AS and McLelland J. London: Academic, 1989, vol. 4, p. 307–368.
133. **Maina JN.** The morphology of a tropical terrestrial slug *Trichotoxon copleyi* (Verdcourt, Mollusca: Gastropoda: Pulmonata). A scanning and transmission electron microscopic study. *J Zool* 217: 355–366, 1989.
134. **Maina JN.** The morphology of the lung of the black mamba, *Dendroapis polylepis* (Reptilia: Ophidia: Elapidae): a scanning and transmission electron microscopic study. *J Anat* 167: 31–46, 1990.
135. **Maina JN.** The morphology of the gills of the African freshwater crab *Potamon niloticus* (Ortmann Crustacea: Brachyura: Potamonidae): a scanning and transmission electron microscopic study. *J Zool* 221: 499–515, 1990.
136. **Maina JN.** A study of the morphology of the gills of an extreme alkalinity and hyperosmotic adapted teleost *Oreochromis alcalicus grahami* (Boulenger) with particular emphasis on the ultrastructure of the chloride cells and their modifications with water dilution: a SEM and TEM study. *Anat Embryol* 181: 83–98, 1990.
137. **Maina JN.** The morphology and morphometry of the lung of the lesser-bushbaby *Galago senegalensis*. *J Anat* 172: 129–144, 1990.
138. **Maina JN.** A morphometric analysis of chloride cells in the gills of the teleosts *Oreochromis alcalicus* and *O. niloticus* and a description of presumptive urea excreting cells in *Oreochromis alcalicus*. *J Anat* 175: 131–145, 1991.
138a. **Maina JN.** Morphometries of the avian lung: the structural-functional correlations in the design of the lungs of birds. *Comp Biochem Physiol A Physiol* 105: 397–410, 1993.
139. **Maina JN.** Comparative pulmonary morphology and morphometry: the functional design of respiratory systems. In: *Advances in Comparative and Environmental Physiology*, edited by Gilles R. Heidelberg, Germany: Springer-Verlag, 1994, vol. 20, p. 111–232.
140. **Maina JN.** *The Gas Exchangers: Structure, Function, and Evolution of the Respiratory Processes*. Heidelberg, Germany: Springer-Verlag, 1998.
140a. **Maina JN.** Comparative morphology: themes and principles in the design and construction of the gas exchangers. *Anat Rec* 261: 24–44, 2000.
140b. **Maina JN.** Location and ultrastructure of podocyte-like phagocytic cells in the gills of a freshwater crab, *Potamon niloticus*–Savigny (Crustacea: Decapoda: Potamonidae): possible implications of diffuse morphologically congruous cell lineage. *Tissue Cell* 30: 562–572, 1998.
141. **Maina JN.** Is the sheet-flow design a "frozen core" (a Bauplan) of the gas exchangers? Comparative functional morphology of the respiratory microvascular systems: illustration of the geometry and rationalization of the fractal properties. *Comp Biochem Physiol A Physiol* 126: 491–515, 2000.
142. **Maina JN.** *Fundamental Structural Aspects in the Bioengineering of the Gas Exchangers: Comparative Perspectives*. Berlin: Springer-Verlag, 2002, p. 112.
143. **Maina JN.** *Functional Morphology of the Vertebrate Respiratory Systems*. Enfield, NH: Science, 2002.
144. **Maina JN.** Some recent advances on the study of the functional design of the avian lung: morphologic and morphometric perspectives. *Biol Rev* 77: 97–152, 2002.
145. **Maina JN.** Structure, function and evolution of the gas exchangers: comparative perspectives. *J Anat* 201: 281–304, 2002.
146. **Maina JN and Cowley HM.** Ultrastructural characterization of the pulmonary cellular defenses in the lung of a bird, the rock dove, *Columba livia*. *Proc R Soc Lond B Biol Sci* 265: 1567–1572, 1998.
147. **Maina JN and King AS.** The thickness of the avian blood-gas barrier: quantitative and quantitative observations. *J Anat* 134: 553–562, 1982.
148. **Maina JN and King AS.** Morphometrics of the avian lung. The wild mallard (*Anas platyrhynchos*) and greylag goose (*Anser anser*). *Respir Physiol* 50: 299–313, 1982.
149. **Maina JN and King AS.** The structural functional correlation in the design of the bat lung. A morphometric study. *J Exp Biol* 111: 43–63, 1984.
150. **Maina JN and King AS.** A morphometric study of the lung of a humboldt penguin *(Spheniscus humboldti)*. *Zentralb Vet Med Anat Histol Embryol* 16: 293–297, 1987.
151. **Maina JN and King AS.** The lung of the emu, *Dromaius novaehollandiae:* a microscopic and morphometric study. *J Anat* 163: 67–74, 1989.
152. **Maina JN, King AS, and King DZ.** A morphometric analysis of the lungs of a species of bat. *Respir Physiol* 50:1–11, 1982.
153. **Maina JN, King AS, and Settle JG.** An allometric study of the pulmonary morphometric parameters in birds, with mammalian comparison. *Philos Trans R Soc Lond B Biol Sci* 326: 1–57, 1989.
154. **Maina JN and Maloiy GMO.** The morphometry of the lung of the lungfish *(Protopterus aethiopicus)*: its structural-functional correlations. *Proc R Soc Lond B Biol Sci* 244: 399–420, 1985.
155. **Maina JN and Maloiy GMO** The morphology of the respiratory organs of the African air-breathing catfish (*Clarias mossambicus*) (Peters): a light, and electron microscopic study, with morphometric observations. *J Zool* 209: 421–445, 1986.

156. **Maina JN and Maloiy GMO.** A scanning and transmission electron microscopic study of the lung of a caecilian, *Boulengerula taitanus*. *J Zool* 215: 739–751, 1988.
157. **Maina JN, Maloiy GMO, and Makanya AN.** Morphology and morphometry of the lungs of two East African mole rats, *Tachyoryctes splendens* and *Heterocephalus glaber* (Mammalia, Rodentia). *Zoomorphology* 112: 167–179, 1992.
158. **Maina JN and Nathaniel C.** A qualitative and quantitative study of the lung of an ostrich, *Struthio camelus*. *J Exp Biol* 204: 2313–2330, 2001.
159. **Maina JN, Thomas SP, and Dallas DM.** A morphometric study of bats of different size: correlations between structure and function of the chiropteran lung. *Philos Trans R Soc Lond B Biol Sci* 333: 31–50, 1991.
160. **Maina JN and van Gil SP.** Morphometric characterization of the airway and vascular systems of the lung of the domestic pig, *Sus scrofa*: comparison of the airway, arterial and venous systems. *Comp Biochem Physiol A Physiol* 130: 781–798, 2001.
161. **Maina JN, Veltcamp CJ, and Henry J.** A study of the spatial organization of the gas-exchange components of a snake lung: the sandboa *Eryx colubrinus* (Reptilia: Ophidia; Corubridae) by latex casting. *J Zool* 247: 81–90, 1999.
162. **Maina JN, Wood CM, Narahara AB, Bergman HL, Laurent P, and Walsh PJ.** Morphology of the swim (air) bladder of a cichlid teleost: *Oreochromis alcalicus grahami* (Trewavas, 1983), a fish adapted to a hyperosmotic, alkaline and hypoxic environment: a brief outline of the structure and function of the swimbladder. In: *Recent Advances in Fish Biology*, edited by Dutta HH and Munshi JSD. New Delhi, India: BHD, 1996, p. 27–45.
163. **McGregor LK, Daniels CB, and Nicholas TE.** Lung ultrastructure and surfactant-like system of the central Australian netted dragon, *Ctenophoruos nuchalis*. *Copeia* 1993: 326–333, 1993.
164. **McKechnie JK, Leart WP, Noakes TD, Kallmeyer JC, MacSearraigh ET, and Oivier LR.** Acute pulmonary oedema in two athletes during a 90-km running race. *S Afr Med J* 56: 261–265, 1979.
165. **Meban C.** Ultrastructure of the respiratory epithelium in the lungs of the newt *Triturus cristatus*. *Acta Zool Stockh* 58: 151–167, 1977.
166. **Meban C.** Functional anatomy of the lungs of the green turtle, *Lacerta viridis*. *J Anat* 125: 421–436, 1978.
167. **Meban C.** An electron microscopy study of the respiratory epithelium in the lungs of the fire salamander (*Salamandra salamandra*). *J Anat* 128: 215–221, 1979.
168. **Meban C.** Thicknesses of the air-blood barriers in vertebrate lungs. *J Anat* 131: 299–307, 1980.
169. **Metcalfe JD and Butler PJ.** The functional anatomy of the gills of the dogfish *(Scyliorhinus canicula)*. *J Zool* 208: 519–530, 1986.
170. **Meyer A and Dolven SI.** Molecules, fossils, and the origin of tetrapods. *J Mol Evol* 35: 102–113, 1992.
171. **Meyrick BL and Reid L.** The alveolar brush cell in rat lung–a third pneumocyte. *J Ultrastruct Res* 23: 71–80, 1968.
172. **Milnor WR.** *Hemodynamics.* Baltimore, MD: Williams & Wilkins, 1982.
173. **Morgan M.** The development of secondary lamellae of the gills of the trout, *Salmo gairdneri* (Richardson). *Cell Tissue Res* 151: 509–523, 1974.
174. **Morrissette N, Gold E, and Aderem A.** The macrophage—a cell for all seasons. *Cell Biol* 9: 199–201, 1999.
175. **Nagaishi CH, Okada Y, Ishiko S, and Daido S.** Electron microscopic observations of the pulmonary alveoli. *Exp Med Surg* 22: 81–97, 1964.
176. **Namba Y, Kurdak SS, Fu Z, Mathieu-Costello O, and West JB.** Effect of reducing alveolar surface tension on stress failure in pulmonary capillaries. *J Appl Physiol* 79: 2114–2121, 1995.
177. **Neal CR and Michel CC.** Openings in frog microvascular endothelium induced by high intravascular pressures. *J Physiol* 492: 39–52, 1996.
178. **Nganpiep L and Maina JN.** Composite cellular defense stratagem in the avian respiratory system: functional morphology of the free (surface) macrophages and specialized pulmonary epithelia. *J Anat* 200: 499–516, 2002.
179. **Okada Y, Ishiko S, Daido S, Kim J, and Ikeda S.** Comparative morphology of the lung with special reference to the alveolar epithelial cells. I. Lungs of Amphibia. *Acta Tuberc Jap* 11: 63–87, 1962.
180. **Olson KR.** Vasculature of the fish gills: anatomical correlates of physiological function. *J Electron Microsc Tech* 2: 217–228, 1991.
181. **Orgeig S and Daniels CB.** The evolutionary significance of pulmonary surfactant in lungfish (Dipnoi). *Am J Respir Cell Mol Biol* 13: 161–166, 1995.
182. **Parker JC, Breen EC, and West JB.** High vascular and airway pressures increase interstitial protein mRNA expression in isolated rat lungs. *J Appl Physiol* 83: 1697–1705, 1997.
183. **Parker JC, Ivey CL, and Tucker JA.** Gadolinium prevents high airway pressure-induced permeability increases in isolated rat lungs. *J Appl Physiol* 84: 1113–1118, 1998.
184. **Parker JC, Townsley MI, and Stevens T.** Ca^{2+} dependence of mechanical injury to lung capillaries. *J Appl Physiol* 86: 775–776, 1999.
185. **Pascoe JR, Ferraro GL, Cannon JH, Arthur RM, and Wheat JD.** Exercise-induced pulmonary hemorrhage in racing thoroughbreds: a preliminary study. *Am J Vet Res* 42: 703–707, 1981.
186. **Pastor LM.** The histology of the reptilian lungs. In: *Histology, Ultrastructure and Immunohistochemistry of Respiratory Organs in Non-Mammalian Vertebrates*, edited by Pastor LM. Murcia, Spain: Publicaciones Universidad de Murcia, 1995, p. 131–153.
187. **Pattle RE.** The lung surfactant in the evolutionary tree. In: *Respiration of Amphibious Vertebrates*, edited by Hughes GM. London: Academic, 1976, p. 233–255.
188. **Perry SF.** Quantitative anatomy of the lungs of the red-eared turtle, *Pseudemys scripta elegans*. *Respir Physiol* 35: 245–262, 1978.
189. **Perry SF.** Reptilian lungs: functional anatomy and evolution. *Adv Anat Embryol Cell Biol* 79: 1–81, 1983.
190. **Perry SF.** Recent advances, and trends in the comparative morphometry of vertebrate gas exchangers. In: *Advances in Comparative and Environmental Physiology. Vertebrate Gas Exchange from Environment to Cell*, edited by Boutilier RG. Berlin: Springer-Verlag, 1990, vol. 6, p. 45–71.
191. **Perry SF.** Gas exchange strategy in the Nile crocodile: a morphometric study. *J Comp Physiol B Biochem Syst Environ Physiol* 159: 761–769, 1990.
192. **Perry SF.** Lungs: comparative anatomy, functional morphology, and evolution. In: *Biology of Reptilia. Morphology*, edited by Gans C and Gaunt AS. Ithaca, NY: Soc. for Study of Amphibians and Reptiles, 1999, vol. 19, p. 1–92.
193. **Perry SF, Hein J, and van Dieke NE.** Gas exchange morphometry of the lungs of the tokay, *Gekko gecko* L. *(Reptilia: Squamata; Gekkonidae)*. *J Comp Physiol B Biochem Syst Environ Physiol* 164: 206–214, 1994.
194. **Pohunkova H and Hughes GM.** Ultrastructure of the lungs of the garter snake. *Folia Morph* 23: 254–258, 1985.
195. **Pough FH, Heiser JB, and McFarland WN.** *Vertebrate Life* (3rd ed.). New York: Macmillan Publishing, 1989.
196. **Power JHT, Doyle IR, Davidson K, and Nicholas TE.** Ultrastructural and protein analysis of surfactant in the Australian lungfish *Neoceratodus forsteri*. *J Exp Biol* 202: 2543–2550, 1999.
197. **Purves WK, Orians GH, Heller HC, and Sadava D.** *Life: The Science of Biology* (4th ed.). San Francisco, CA: Freeman, 1997.
198. **Randall DJ.** The control of respiration and circulation in fish during exercise and hypoxia. *J Exp Biol* 100: 275–288, 1982.
199. **Reeves JT, Groves BM, Cymerman A, Sutton Wagner PD, Turkevich D Jr, and Houston CS.** Operation Everest II: cardiac filling pressures during cycle exercise at sea level. *Respir Physiol* 80: 147–154, 1990.
200. **Roughton FJW and Forster RE.** Relative importance of diffusion and chemical reaction rates in determining rate of exchange of gases in the human lung, with special reference to true diffusing capacity of pulmonary membrane and volume of blood in the lung capillaries. *J Appl Physiol* 11: 290–302, 1957.
201. **Savige J, Rana K, Tonna S, Buzza M, Dagher H, and Wang YY.** Thin basement membrane nephropathy. *Kidney Int* 64: 1169–1178, 2003.
202. **Schneeberger-Keeley EE and Karnovsky MJ.** The ultrastructural basis of alveolar-capillary membrane permeability to peroxidase used as a tracer. *J Cell Biol* 37: 781–793, 1968.

203. **Schoene RB, Hackett PH, Henderson WR, Sage EH, Chow M, Roach RC, Mills WJ, and Martin TR.** High-altitude pulmonary edema. Characteristics of lung lavage fluid. *J Am Med Assoc* 256: 63–69, 1986.
204. **Schuger L, Skutitz APN, O'Shea S, Chang JF, and Varani J.** Identification of laminin domains involved in branching morphogenesis: effects of antilaminin monoclonal antibodies on mouse embryonic lung development. *Dev Biol* 146: 531–541, 1991.
205. **Schwartz U, Schuppan D, Oberbaumer I, Glansville R, Deutzmann R, Timpl R, and Kuhn K.** Structure of mouse type IV collagen. Amino-acid sequence of the C-terminal 511-residue-long triple-helical segment of the alpha 2(IV) chain and its comparison with the alpha 1(IV) chain. *Eur J Biochem* 157: 49–56, 1986.
206. **Sebring RJ and Lehnert BE.** Morphometric comparisons of rat alveolar macrophages, pulmonary interstitial macrophages, and blood monocytes. *Exp Lung Res* 18: 479–496, 1992.
207. **Sibley CG and Alhquist JE.** *Phylogeny and Classification of Birds: A Study in Molecular Evolution.* New Haven, CT: Yale Univ. Press, 1990.
208. **Skalak R and Chien S.** *Handbook of Bioengineering*. New York: McGraw-Hill, 1987.
209. **Smith DG and Chamley-Campbell J.** Localization of smooth muscle myosin in branchial pillar cells of snapper, *Chrysophys auratus*, by immunofluorescence histochemistry. *J Exp Biol* 215: 121–124, 1981.
210. **Sparti A.** Thermogenic capacity of shrews (Mammalia, Soricidae), and its relationship with basal rate of metabolism. *Physiol Zool* 65: 77–96, 1992.
211. **Staub NC.** The pathophysiology of pulmonary edema. *Human Pathol* 1: 419–432, 1970.
212. **Stenmark KR and Mecham RP.** Cellular and molecular mechanisms of pulmonary vascular remodeling. *Annu Rev Physiol* 59: 89–144, 1997.
213. **Stinner JN.** Functional anatomy of the lung of the snake, *Pituophis melanoleucus*. *Am J Physiol Regul Integr Comp Physiol* 243: R251–R257, 1982.
214. **Stromberg DD and Wiederhielm CA.** Viscoelastic description of a collagenous tissue in simple elongation. *J Appl Physiol* 26: 857–862, 1969.
215. **Sullivan LC, Daniels CB, Phillips ID, Orgeig S, and Whitsett JA.** Conservation of surfactant protein A: evidence for a single origin for vertebrate pulmonary surfactant. *J Mol Evol* 46: 131–138, 1998.
216. **Swayne GT, Smaje LH, and Bergel DH.** Distensibility of single capillaries and venules in the rat and frog mesentery. *Int J Microcirc Clin Exp* 8: 25–42, 1989.
217. **Szidon JP, Pietra GG, and Fishman AP.** The alveolar-capillary membrane and pulmonary edema. *N Engl J Med* 286: 1200–1204, 1972.
218. **Takami H, Burbelo PD, Fukuda K, Chang HS, Phillips SL, and Yamada Y.** Molecular organization and gene regulation of type IV collagen. *Contrib Nephrol* 107: 36–46, 1994.
219. **Tappan H.** Molecular evoltion. In: *Molecular Oxygen in Biology*, edited by Hayaishi O. Amsterdam: Elsevier-North Holland, 1974, p. 81–135.
220. **Thompson KS.** The biology of the lobe-finned fishes. *Biol Rev* 44: 91–154, 1969.
221. **Timpl R, Wiedemann H, van Delden V, Furthmayr H, and Kühn K.** A network model for the organization of type IV collagen molecules in basement membranes. *Eur J Biochem* 120: 203–211, 1981.
222. **Torday JS and Rehan VK.** Deconvoluting lung evolution using functional/comparative genomics. *Am J Respir Cell Mol Biol* 31: 8–12, 2004.
223. **Tsukimoto K, Mathieu-Costello O, Prediletto R, Elliot AR, and West JB.** Ultrastructural appearances of pulmonary capillaries at high transmural pressures. *J Appl Physiol* 71: 573–582, 1991.
224. **Untersee P, Gil J, and Weibel ER.** Diffusion capacity in rat lungs fixed at different degrees of inflation. *Experientia* 28: 732–742, 1972.
225. **Vaccaro CA and Brody JS.** Structural features of alveolar wall basement membrane in the adult rat lung. *J Cell Biol* 91: 427–437, 1981.
226. **Vidyadaran MK, King AS, and Kassim H.** Deficient anatomical capacity for oxygen uptake of the developing lung of the female domestic fowl when compared with red-jungle fowl. *Schw Archiv Tier* 129: 225–237, 1987.
227. **Wagner GP.** The origin of morphological characters and the biological basis of homology. *Evolution* 43: 1157–1171, 1989.
228. **Wagner GP.** Complexity matters. *Science* 279: 1158–1159, 1998.
229. **Wagner PD, Gale GE, Moon RE, Torre-Bueno JR, Stolp BW, and Saltzman HA.** Pulmonary gas exchange in humans exercising at sea level and simulated altitude. *J Appl Physiol* 61: 260–270, 1986.
230. **Weibel ER.** *Morphometry of the Human Lung.* Berlin: Springer-Verlag, 1963.
231. **Weibel ER.** Principles and methods for the morphometric study of the lung and other organs. *Lab Invest* 12: 131–155, 1963.
232. **Weibel ER.** Morphometric estimation of pulmonary diffusion capacity. I. Model and method. *Respir Physiol* 11: 54–75, 1970.
233. **Weibel ER.** Morphological basis of the alveolar-capillary gas exchange. *Physiol Rev* 53: 419–495, 1973.
234. **Weibel ER.** *The Pathway for Oxygen.* Cambridge, MA: Harvard Univ. Press, 1984.
235. **Weibel ER.** Lung cell bology. In: *Handbook of Physiology. The Respiratory System. Circulation and Nonrespiratory Functions.* Bethesda, MD: Am. Physiol. Soc., 1985, sect. 3, vol. I, chapt. 2, p. 47–91.
236. **Weibel ER.** Functional morphology of the lung parenchyma. In: *Handbook of Physiology. The Respiratory System. Mechanics of Breathing.* Bethesda, MD: Am. Physiol. Soc., 1986, sect. 3, vol. III, pt. 1, chapt. 8, p. 89–111.
237. **Weibel ER.** Lung morphometry and models in respiratory physiology. In: *Respiratory Physiology: An Analytical Approach*, edited by Chang HK and Paiva M. New York: Dekker, 1989, p. 1–55.
238. **Weibel ER.** The structural basis of lung function. In: *Respiratory Physiology: People and Ideas*, edited by West JB. New York: Oxford Univ. Press, 1996, p. 3–46.
239. **Weibel ER.** *Symmorphosis: On Form, and Function in Shaping Life.* Cambridge, MA: Harvard Univ. Press, 2000.
240. **Weibel ER, Federspiel WJ, Fryder-Doffey F, Hsia CW, König M, Stalder-Navarr VM, and Vock R.** Morphometric model for pulmonary diffusing capacity I Membrane diffusing capacity. *Respir Physiol* 93: 125–149, 1993.
241. **Weibel ER and Knight BW.** A morphometric study of the thickness of the pulmonary air-blood barrier. *J Cell Biol* 21: 367–384, 1964.
242. **Weiler-Ravell D, Shupak A, Goldberg I, Halpem P, Shoshani O, Hirschhom G, and Margulis A.** Pulmonary oedema and haemoptysis induced by strenuous swimming. *Br Med J* 311: 361–362, 1995.
243. **Welling LW and Grantham JJ.** Physical properties of isolated perfused renal tubules and tubular basement membranes. *J Clin Invest* 51: 1063–1075, 1972.
244. **Welsch U.** Phagocytosis in the amphibian lung. *Anat Anz* 154: 323–327, 1983.
245. **Welsch U and Aschauer B.** Ultrastructural observations on the lung of the emperor penguin (*Aptenodytes forsteri*). *Cell Tissue Res* 243: 137–144, 1986.
246. **West JB.** *Respiratory Physiology: The Essentials.* Baltimore, MD: Williams & Wilkins, 1974.
247. **West JB.** Cellular responses to mechanical stress: pulmonary capillary stress failure. *J Appl Physiol* 89: 2483–2489, 2000.
248. **West JB.** Thoughts on the pulmonary blood-gas barrier. *Am J Physiol Lung Cell Mol Physiol* 285: L501–L513, 2003.
249. **West JB and Mathews FL.** Stresses, strains, and surface pressures in the lung caused by its weight. *J Appl Physiol* 32: 332–345, 1978.
250. **West JB and Mathieu-Costello O.** Strength of the pulmonary blood-gas barrier. *Respir Physiol* 88: 141–148, 1992.
251. **West JB and Mathieu-Costello O.** Structure, strength, failure, and remodeling of the pulmonary blood-gas barrier. *Annu Rev Physiol* 61: 543–572, 1999.
252. **West JB, Mathieu-Costello O, Jones JH, Birks EK, Logerman RB, Pascoe JR, and Tyler WS.** Stress failure of pulmonary cap-

illaries in racehorses with exercise-induced pulmonary hemorrhage. *J Appl Physiol* 75: 1097–1109, 1993.
253. **West JB, Tsukimoto K, Mathieu-Costello O, and Prediletto R.** Stress failure in pulmonary capillaries. *J Appl Physiol* 70: 1731–1742, 1991.
254. **Whitwell KE and Greet TR.** Collection and evaluation of tracheobronchial washes in the horse. *Equine Vet J* 16: 499–508, 1984.
255. **Wienner F, Morkin E, Skalak R, and Fishman AP.** Wave propagation in the pulmonary circulation. *Circ Res* 19: 834–850, 1966.
256. **Wieslander J and Heinegard D.** The involvement of type IV collagen in Goodpasture's Syndrome. *Ann NY Acad Sci* 460: 363–374, 1985.
257. **Williamson JR, Vogler NJ, and Kilo C.** Regional variations in the width of the basement membrane of muscle capillaries in man and giraffe. *Am J Pathol* 63: 359–370, 1971.
258. **Yakobori S, Hasegawa M, Ueda T, Okada N, Nishikawa K, and Watanabe K.** Relation among coelacanths, lungfishes, and tetrapods: a phylogenetic analysis based on mitochondrial cytochrome oxidase I gene sequences. *J Mol Evol* 38: 602–609, 1994.
259. **Yamada H.** *Strength of Biological Materials*. Baltimore, MD: Williams & Wilkins, 1970.
260. **Zardoya R and Meyer A.** The complete nucleotide sequence of the mitochondrial genome of the lungfish (*Protopterus dolloi*) supports its phylogenetic position as a close relative of land vertebrates. *Genetics* 142: 1249–1263, 1996.
261. **Zardoya R and Meyer A.** Molecular phylogenetic information on the identity of the closest living relative(s) of land animals. *Naturwissenschaften* 84: 389–397, 1997.